Brodogradnja Volume 77 Number 4 (2026) 77409

University of Zagreb
Faculty of Mechanical
Engineering and Naval
Architecture

journal homepage: www.brodogradnja.fsb.hr

Brodogradnja

An International Journal of Naval Architecture and
Ocean Engineering for Research and Development

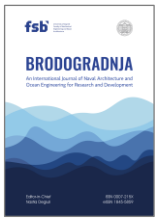

An adaptive predefined time trajectory tracking control approach for unmanned surface vehicles under short-crested wave disturbances

Zhiyang Guo[1], *Jianing Zhang*[1,*], *Yuchen Shang*[2], *Yi Zhang*[1], *Yuanhui Wei*[1], *Lei Zhang*[1]

[1]*School of Naval Architecture and Ocean Engineering, Dalian Maritime University, Dalian 116026, China*
[2]*Department of Ocean Engineering, Texas A&M University, College Station 77843, USA*

ARTICLE INFO

Keywords:
Predefined time
Adaptive control
Unmanned surface vehicle
Trajectory tracking
Short-crested waves

ABSTRACT

This paper focuses on trajectory tracking control problem in unmanned surface vehicles (USVs) operating under complex ocean disturbances. To accurately characterize the marine environment and evaluate control performance under realistic operating conditions, a three-dimensional short-crested irregular wave force model with randomly distributed frequencies and propagation directions is established. This model incorporates stochastic and multidirectional wave loading into the USV dynamics and control framework, providing a more realistic representation of wave disturbances for trajectory tracking analysis. Building upon this disturbance modeling, an adaptive predefined time nonsingular terminal sliding mode controller (adaptive PT-NTSMC) is proposed. First, a novel time-varying function is introduced to construct a variable-gain global sliding mode manifold, based on which a predefined time controller is developed to ensure predefined time convergence. Second, an adaptive law is established to independently estimate the upper bound of external disturbances, thereby reducing the reliance of controller design on prior disturbance-bound information. The global and predefined time stability of the closed-loop system is rigorously verified using Lyapunov theory. Simulation and comparative results under short-crested wave conditions validate the effectiveness and improved performance of the proposed control strategy.

1. Introduction

In recent years, with the increasing scarcity of land resources, the development and utilization of marine resources have become particularly important. In this context, unmanned surface vehicles (USVs) have garnered significant attention as essential tools for marine exploration. During the navigation of USVs, the primary external disturbance arises from wave forces acting on the sea surface. Therefore, establishing an accurate hydrodynamic model of wave forces is essential for improving the fidelity of numerical simulations, enhancing the reliability of simulation results, and improving the practical applicability of controller parameters. The influence of wave forces on USVs mainly consists of two components: the first-order wave force, which primarily excites oscillatory motions such as heave, roll, and pitch, and the second-order wave

* Corresponding author.
E-mail address: zhangjianing@dlmu.edu.cn

https://doi.org/10.21278/brod77409
Received 26 February 2026; Received in revised 06 May 2026; Accepted 20 May 2026
Available online 03 June 2026
ISSN 0007-215X; eISSN 1845-5859

drift force, which causes slow variations or drifts in the USV position. However, in most existing studies, researchers have simulated wave disturbances by simply superimposing sinusoidal and cosine functions [1-3], and this approach fails to capture the physical characteristics of real ocean wave forces. In some works, long-crested irregular wave models based on wave spectra [4] have been employed, which partially reflect the distribution of wave energy across different frequencies. Nevertheless, such models essentially describe two-dimensional planar waves and cannot represent the effects of multidirectional component waves on the resultant wave forces. Moreover, since the heading and speed of a USV change continuously during motion, the use of a two-dimensional wave model may lead to unrealistic results—for instance, the force components in certain degrees of freedom may become zero when the USV heading coincides with specific wave propagation angles. In addition, the selection of component wave frequencies significantly affects the computed wave forces when spectral representations are used. Although evenly spaced frequency discretization simplifies the computation, it tends to produce periodic repetitions in the simulated wave forces, leading to deviations from the stochastic and nonrepetitive characteristics of actual ocean environments. Therefore, it is necessary to establish an accurate and physically consistent wave force model that not only improves simulation fidelity but also provides a solid foundation for analyzing and compensating for external disturbances in control design.

Achieving accurate trajectory tracking under complex environmental disturbances has become a prominent focus in research in recent years. Many researchers have explored various control methods with promising results. Currently, widely used approaches include proportional–integral–derivative (PID) control [5], sliding mode control (SMC) [6], model predictive control (MPC) [7], fuzzy logic control (FLC) [8], backstepping [9], neural-network-based control [10], and reinforcement learning (RL) [11, 12]. Among these methods, PID control has a simple structure and is easy to implement but lacks robustness against nonlinearities and external disturbances. It also exhibits slow dynamic responses and lower tracking accuracy in nonlinear systems. MPC provides good tracking performance for smooth trajectories but struggles with sharp turns and small-angle trajectories. Its robustness depends on the accuracy of the system model, and its convergence speed is often slower than that of SMC because of the complexity of solving optimization problems. Compared with SMC, FLC offers strong robustness but relies on manually designed fuzzy rules, making it less effective at handling complex dynamic variations and unknown disturbances. The backstepping method is less robust in handling rapidly changing system dynamics and strong disturbances, but its tracking performance for sharp turns is slightly inferior to that of SMC. In contrast, SMC has stronger robustness, faster convergence, and higher tracking accuracy for complex trajectories, making it the mainstream approach in controller design [13-15]. In recent years, many researchers have integrated SMC with other advanced control techniques to improve trajectory tracking performance [16-19].

Another important issue in trajectory tracking control lies in a system's convergence behavior. For autonomous marine vehicles (AMVs), achieving stable tracking within a specified time is a key performance criterion. Accordingly, minimizing the pursuit phase duration while maintaining tracking accuracy remains a central focus in trajectory tracking control research. The research on system convergence time can be broadly classified into four stages: asymptotic stability, finite-time stability, fixed-time stability, and predefined time stability. Asymptotic stability has been studied for more than a century. However, since an asymptotically stable system can only approach the equilibrium point infinitely as time tends to infinity, it fails to meet the requirements for time-constrained control applications. Finite-time stability requires that the system states converge to the equilibrium point within a finite time horizon [20, 21]. Because finite time stability is associated with faster dynamic response than asymptotic stability, it has been widely applied in the control of unmanned systems. For the trajectory tracking of fully actuated USVs, the authors of references [22-25] developed a nonsingular fast terminal sliding mode controller, a supertwisting sliding mode controller, a PID sliding mode controller, and a nonlinear sliding mode controller. However, the parameter design of these controllers or observers relies on the upper bound of the disturbance derivative, the disturbance bound, or lumped terms containing disturbances. In reference [26], an improved finite-time convergent LOS method was proposed. Although the controller itself does not explicitly depend on disturbance information, the convergence region of the tracking error is still jointly affected by the control parameters and external disturbances. In references [27] and [28], adaptive fuzzy control and reinforcement-learning-based adaptive

control, respectively, were introduced to improve tracking accuracy, robustness, and energy efficiency. Overall, the above finite-time control methods generally rely on prior disturbance-related information for parameter design or performance assurance. Moreover, their convergence time depends on the initial conditions. Specifically, a larger initial deviation leads to a longer actual convergence time.

Fixed-time stability guarantees that the system states converge to the equilibrium point within a uniform upper time bound independent of the initial conditions [29, 30], and thus exhibits greater advantages in control tasks that require unified time constraints. In recent years, the fixed time framework has been widely applied in AMV trajectory tracking, formation control, dynamic positioning, and autonomous berthing. Among these works, the authors of references [31-33] achieved fixed time convergence via disturbance observers or SMC, but parameter design still required consideration of the upper bound of the disturbance or its derivative. Although the authors of references [34] and [35] alleviated some of the drawbacks of conventional methods to a certain extent, their observation or tracking error bounds continue to be jointly influenced by the controller parameters magnitude of disturbance. References [36], [37], and [38] reduced the reliance on disturbance-bound information through neural-network approximation or dynamic compensation mechanisms. In reference [39], a fixed time fuzzy adaptive backstepping controller was designed for the cooperative formation tracking control of fully actuated USVs, ensuring that the tracking errors converge to a neighborhood of the origin within a fixed time period. Reference [40] proposed a fixed-time fault-tolerant control scheme for unmanned amphibious surface vehicles with actuator faults, providing an effective solution for maintaining trajectory-tracking performance in the presence of actuator faults and uncertainties. However, the method still relies on prior boundedness information on the lumped disturbance and its time derivative. In contrast, reference [41] considered only system uncertainties and did not consider external disturbances. In general, although the above fixed-time control methods eliminate the dependence on initial conditions, their upper convergence-time bounds are still related to the controller parameters. When the controller structure becomes complicated and the number of parameters increases, such upper bounds are often difficult to specify directly and precisely in advance.

On this basis, the predefined time stability approach further allows the convergence time to be treated as an independently assignable parameter, such that the convergence time is not only independent of the initial conditions but also decoupled from the complicated coupling relationships among other control parameters [42, 43]. Therefore, the predefined time stability approach provides a more direct and effective theoretical framework for control tasks subject to strict time requirements and has gradually become an important direction in current research. In recent years, predefined time methods have been applied to the coordinated control of networked marine surface vessels, data-driven trajectory tracking of hovercraft, and formation control of multiple AUVs [44-46], with favorable time-constrained performance. The authors of reference [47] further constructed a hybrid framework for prescribed-time trajectory tracking control of an aquatic-aerial unmanned amphibious vehicle under actuator faults, thereby extending the application of time-constrained control to more complex task scenarios. However, in existing studies, the parameter design of controllers or observers still often depends on disturbance bounds, which to some extent limits their practical applicability.

In this paper, predefined time stability refers to a convergence property in which the actual convergence time of the system is bounded by an upper bound that can be assigned in advance by the designer and remains independent of the initial condition. More specifically, the adopted notion mainly requires a unified and adjustable upper bound on the actual convergence time. Therefore, even if certain auxiliary parameters are determined with the aid of initial-condition information during the controller construction, the predefined time property is still maintained, provided that the designer-assigned convergence time bound itself does not depend on the initial state. In the proposed method, the predefined time parameter is chosen in advance, whereas the initial conditions are only used to determine the auxiliary parameter vector and gain term involved in the sliding manifold construction, such that the prescribed initial constraints of the manifold are satisfied. In other words, variations in the initial conditions do not influence the convergence time of the system. Since these quantities are introduced only for structural construction and do not affect the designer-assigned convergence time bound, the predefined time convergence claim of the proposed method remains valid under the adopted definition.

Table 1 Comparison of the disturbance handling and convergence characteristics of existing AMV control methods

Ref	disturbance model	Whole-process disturbance-bound information required	Convergence type
[4]	Long-Crested Wave	No	asymptotic
[22-25]	Sinusoidal composite disturbance	Yes	Finite time
[26-28]		No	
[31, 32]	Sinusoidal composite disturbance	Yes	Fixed time
[36-38]		No	
[39]	Gaussian white noise		
[44-46]	Sinusoidal composite disturbance	Yes	Predefined time
This paper	Short-Crested Wave	No	

In summary, several issues still remain to be addressed in USV tracking control.

First, the disturbance-force models used to describe the operating environment of USVs are often overly simplified, making it difficult to adequately capture the physical characteristics of external disturbances and thereby reducing the reliability of simulation results.

Second, the research on predefined time control for USVs is still relatively limited. In the existing predefined time sliding mode controllers, effective disturbance suppression is often lacking during the reaching phase, which makes the control algorithm relatively sensitive to external disturbances in the initial stage.

Third, parameter selection in most existing predefined time controllers still depends on disturbance-bound information. Moreover, the corresponding control parameters are usually active throughout the entire control process. As a result, the disturbance bound over the whole operating cycle of the USV must be considered during parameter design, which reduces the practical applicability of these algorithms in real-world scenarios.

To address the above issues, in this paper, we develop a control framework that combines a more realistic environmental disturbance model with a predefined time control strategy that further reduces the dependence on disturbance-related prior information. The main contributions of this paper are as follows:

i. A realistic short-crested irregular wave force model is established to accurately simulate environmental disturbances acting on a USV. Nonuniformly spaced component wave frequencies are randomly selected within each interval, and the corresponding propagation directions are generated to reflect the stochastic nature of sea states. This modeling strategy avoids the periodic artifacts that commonly occur in frequency-discretized wave simulations and provides a more faithful representation of the spatial and temporal variability of real ocean wave forces. Moreover, by embedding this physically representative wave force model directly into the USV motion and control framework, the proposed approach enables control design and performance evaluation under physically consistent, multidirectional wave disturbances, which significantly enhances the realism and credibility of control-oriented simulations.

ii. On the basis of a novel time-varying function, a variable-gain predefined-time sliding mode manifold is constructed, and a predefined-time nonsingular terminal sliding mode controller is subsequently developed. By introducing the time-varying function into the sliding manifold, the proposed design guarantees predefined-time stability while simultaneously achieving the global sliding property, thereby eliminating the reaching phase. Furthermore, a variable-gain coefficient is incorporated so that, as the tracking error decreases, the controller can still drive the system toward the desired trajectory at a relatively fast rate.

iii. An adaptive predefined time control scheme is proposed, in which an online estimation law for determining the upper bound of the disturbance is embedded into the predefined time sliding-mode

framework, ensuring that both the tracking error and the upper-bound estimation error converge within a predefined time. Since the related control parameters only take effect before the predefined time, their design only needs to account for the disturbance bound over this interval, rather than over the entire operating cycle as required in many existing methods.

The structure of this paper is as follows. In Section 2, the 3DOF motion model of the USV is introduced, along with the necessary assumptions and lemmas for stability analysis. In Section 3, the modeling of ocean disturbances is presented, where the first- and second-order wave forces induced by three-dimensional short-crested irregular waves are incorporated. In Section 4, the mathematical model of the predefined time nonsingular terminal sliding mode controller is presented, and its stability is proven. On this basis, an adaptive predefined time controller is designed, and its stability is verified using Lyapunov theory. In Section 5, the proposed controller is compared with existing SMC methods, and its performance is analyzed under different initial conditions and various time parameters. Finally, Section 6 presents the conclusions.

Notation: Let $x=[x_1,x_2,\cdots,x_n]^{\mathrm{T}}$ and $y=[y_1,y_2\cdots y_n]^{\mathrm{T}}$ be vectors and let $\beta>0$ be a constant. The Hadamard product of x and y is defined as $x\circ y=[x_1y_1,x_2y_2,\cdots x_ny_n]^{\mathrm{T}}$. Let $x^{\beta}=\left[x_1^{\beta},x_2^{\beta},\cdots,x_n^{\beta}\right]^{\mathrm{T}}$, $|x|=\left[|x_1|,|x_2|,\cdots,|x_n|\right]^{\mathrm{T}}$, $|x|^{\beta}=\left[|x_1|^{\beta},|x_2|^{\beta},\cdots,|x_n|^{\beta}\right]^{\mathrm{T}}$, $\frac{1}{x}=\left[\frac{1}{x_1},\frac{1}{x_2},\cdots,\frac{1}{x_n}\right]^{\mathrm{T}}$, $\mathrm{sig}^{\beta}(x)=|x|^{\beta}\circ\mathrm{sign}(x)$, $x+\beta=[x_1+\beta,x_2+\beta,\cdots,x_n+\beta]^{\mathrm{T}}$, $\mathrm{diag}(x)=\mathrm{diag}(x_1,x_2,\cdots,x_n)$. The Euclidean 2-norm is denoted by $\|*\|$, and the Euclidean 1-norm is denoted by $\|*\|_1$.

2. Problem formulation and preliminaries

2.1 Problem formulation

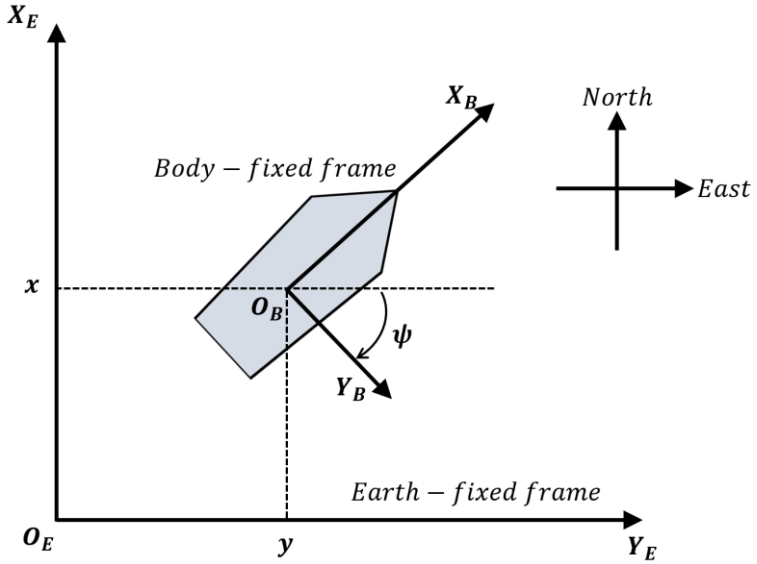

Fig.1 USV 3-DOF planar motion coordinate system

The trajectory tracking problem relates primarily to the position of the USV; thus, the degrees of freedom related to pitch, heave, and roll are typically ignored. The 3-DOF motion coordinate system of a USV is shown in Figure 1. It should be noted that the USV considered in this study is modeled as a fully actuated planar 3-DOF platform, that is, independent control inputs are assumed to be available in the surge, sway, and yaw. The mathematical model for the 3-DOF motion of a USV can be expressed as follows [48]:

$$\begin{aligned}&\dot{\eta}=R(\psi)\upsilon\\&M\dot{\upsilon}+C(\upsilon)\upsilon+D(\upsilon)\upsilon=\tau_c(t)+d(t)\end{aligned}\tag{1}$$

where $\eta=[x,y,\psi]^{\mathrm{T}}$ is the position vector of the USV in the earth-fixed coordinate system; $\upsilon=[u,v,r]^{\mathrm{T}}$ is the velocity vector of the USV in the body-fixed coordinate system; $\tau_c=\left[\tau_x,\tau_y,\tau_\psi\right]^{\mathrm{T}}$ represents the control inputs of the fully actuated USV; $d=[d_1,d_2,d_3]^{\mathrm{T}}$ denotes the unknown disturbance forces in the three degrees of freedom; $R(\psi)$ is the transformation matrix from the body-fixed coordinate system to the earth-fixed coordinate system.

$$R(\psi)=\begin{bmatrix}\cos\psi & -\sin\psi & 0\\ \sin\psi & \cos\psi & 0\\ 0 & 0 & 1\end{bmatrix}\tag{2}$$

$R(\psi)$ has the following properties: $\det R(\psi)=\left\|R(\psi)\right\|=1$; $R^{\mathrm{T}}(\psi)R(\psi)=I$; $\dot{R}(\psi)=R(\psi)S(r)$, where $S(r)=\begin{bmatrix}0 & -r & 0\\ r & 0 & 0\\ 0 & 0 & 0\end{bmatrix}$.

$M,C(\upsilon),D(\upsilon)$ denote the inertia matrix, the Coriolis and centripetal matrix, and the damping matrix, respectively. Their expressions are given as follows:

$$M=\begin{bmatrix}m_{11} & 0 & 0\\ 0 & m_{22} & m_{23}\\ 0 & m_{32} & m_{33}\end{bmatrix}\tag{3}$$

$$C(\upsilon)=\begin{bmatrix}0 & 0 & c_{13}(v,r)\\ 0 & 0 & c_{23}(u)\\ c_{31}(v,r) & c_{32}(u) & 0\end{bmatrix}\tag{4}$$

$$D(\upsilon)=\begin{bmatrix}d_{11}(u) & 0 & 0\\ 0 & d_{22}(v,r) & d_{23}(v,r)\\ 0 & d_{32}(v,r) & d_{33}(v,r)\end{bmatrix}\tag{5}$$

where $m_{11}=m-X_{\dot{u}}$, $m_{22}=m-Y_{\dot{v}}$, $m_{23}=mx_G-Y_{\dot{r}}$, $m_{32}=mx_G-N_{\dot{v}}$, $m_{33}=I_z-N_{\dot{r}}$, $c_{13}(v,r)=-m_{22}v-m_{23}r$, $c_{23}(u)=m_{11}u$, $c_{31}(v,r)=-c_{13}(v,r)$, $c_{32}(u)=-c_{23}(u)$, $d_{11}(u)=-X_u-\left(X_{|u|u}|u|+X_{uuu}u^2\right)$, $d_{22}(v,r)=-Y_v-\left(Y_{|v|v}|v|+Y_{|r|v}|r|\right)$, $d_{23}(v,r)=-Y_r-\left(Y_{|v|r}|v|+Y_{|r|r}|r|\right)$, $d_{32}(v,r)=-N_v-\left(N_{|v|v}|v|+N_{|r|v}|r|\right)$, $d_{33}(v,r)=-N_r-\left(N_{|v|r}|v|+N_{|r|r}|r|\right)$. The parameters m_{ij} , c_{ij} , and d_{ij} denote the elements of the corresponding coefficient matrices in the actual model, while m'_{ij}, c'_{ij}, and d'_{ij}denote the elements of the corresponding nominal coefficient matrices. The terms Δm_{ij}, Δc_{ij}, and Δd_{ij}represent the variations of the unknown parameters. Therefore, the following relationships hold: $m_{ij}=\Delta m_{ij}+m'_{ij}$, $c_{ij}=\Delta c_{ij}+c'_{ij}$, $d_{ij}=\Delta d_{ij}+d'_{ij}$.

Based on Equation (1), the USV dynamics can be reformulated in the earth-fixed coordinate system as follows:

$$\bar{M}(\eta)\ddot{\eta}+\bar{C}(\upsilon,\eta)\dot{\eta}+\bar{D}(\upsilon,\eta)\dot{\eta}=R(\psi)\tau_c(t)+\bar{d}(t) \tag{6}$$

where $\bar{M}(\eta)=R(\psi)MR^{-1}(\psi)$, $\bar{C}(\upsilon,\eta)=R(\psi)C(\upsilon,\eta)R^{-1}(\psi)-R(\psi)MR^{-1}(\psi)\dot{R}(\psi)R^{-1}(\psi)$, $\bar{D}(\upsilon,\eta)=R(\psi)D(\upsilon)R^{-1}(\psi)$, $\bar{d}(t)=R(\psi)d(t)$.

In practical applications, the USV model parameters are not strictly constant because of equipment aging, installation deviations, and environmental variations. Moreover, hydrodynamic effects during navigation may cause the actual coefficient matrices to differ from the nominal ones used in controller design. Therefore, parameter uncertainties and external disturbances are incorporated into the model. Let $*_n$ denote the nominal parameter matrix and $*_u$ represent the parameter error matrix resulting from uncertainties. The relationships among the actual parameter matrix, the nominal parameter matrix, and the parameter error matrix can be expressed as follows: $\bar{M}(\eta)=\bar{M}_n(\eta)+\bar{M}_u(\eta)$, $\bar{C}(\upsilon,\eta)=\bar{C}_n(\upsilon,\eta)+\bar{C}_u(\upsilon,\eta)$, $\bar{D}(\upsilon,\eta)=\bar{D}_n(\upsilon,\eta)+\bar{D}_u(\upsilon,\eta)$.

Thus, Equation (6) can be rewritten as:

$$\bar{M}_n(\eta)\ddot{\eta}+\bar{C}_n(\upsilon,\eta)\dot{\eta}+\bar{D}_n(\upsilon,\eta)\dot{\eta}=R(\psi)\tau_c(t)+\bar{d}_l(t,\upsilon,\eta) \tag{7}$$

where $\bar{d}_l(t,\upsilon,\eta)=\bar{d}(t)-\bar{M}_u(\eta)\ddot{\eta}-\bar{C}_u(\upsilon,\eta)\dot{\eta}-\bar{D}_u(\upsilon,\eta)\dot{\eta}$ represents the lumped disturbance acting on the system.

In the earth-fixed coordinate system, the position and velocity tracking errors are introduced as $\eta_e=\eta-\eta_d$ and $\omega_e=\omega-\omega_d=\dot{\eta}-\dot{\eta}_d$, respectively, where $\eta_d=[\eta_{d1},\eta_{d2},\eta_{d3}]^{\mathrm{T}}$ represents the target trajectory. The second-order derivative of the position error can be expressed as:

$$\dot{\omega}_e=\ddot{\eta}-\ddot{\eta}_d=\bar{M}_n^{-1}(\eta)\left(R(\psi)\tau_c(t)+\bar{d}_l(t,\upsilon,\eta)-\bar{C}_n(\upsilon,\eta)\dot{\eta}-\bar{D}_n(\upsilon,\eta)\dot{\eta}\right)-\ddot{\eta}_d \tag{8}$$

2.2 Preliminaries

Assumption 1 [49] : The desired trajectory is assumed to be smooth, with bounded first and second-order derivatives.

Assumption 2 [50]: The external disturbances are bounded, and the required control input does not persistently exceed the actuator saturation limits. Equivalently, the actuator may experience temporary saturation, but it is not forced to remain continuously saturated throughout the control process. Under this feasibility condition, the upper bound of the lumped disturbance is assumed to satisfy:

$$\| \tau_d \| < \lambda_0+\lambda_1 \| v \| +\lambda_2 \| v \|^2 \tag{9}$$

where, λ_0, λ_1, λ_2 are positive constants.

On this basis, since $R(\psi)$ and its inverse $R^{-1}(\psi)$ have the following properties: $\left\|R(\psi)\right\|=r_0$, $\left\|R^{-1}(\psi)\right\|=r_0$, $r_0=1$. According to the kinematic equation, $\upsilon=R^{-1}(\psi)\dot{\eta}$. We have $\|\upsilon\|\le\left\|R^{-1}(\psi)\right\|\|\dot{\eta}\|$. Therefore, Equation (9) can be rewritten as follows:

$$\| \bar{d}_l(t,\upsilon,\eta) \| < l_0+l_1 \| \dot{\eta} \| +l_2 \| \dot{\eta} \|^2 \tag{10}$$

where $\bar{d}_l(t,\upsilon,\eta)=\tau_d$, $l_0=\lambda_0$, $l_1=\lambda_1$, $l_2=\lambda_2$.

Equation (10) can be further rewritten in the following form:

$$\left\|\bar{d}_l(t,\upsilon,\eta)\right\|\le l_0+l_1\|\dot{\eta}\|+l_2\|\dot{\eta}\|^2\le D_l \quad D_l=l\mathrm{H} \tag{11}$$

where $l_0 \geq 0$, $l_1 \geq 0$, $l_2 \geq 0$, $l = \max(l_0, l_1, l_2)$, $\mathrm{H} = 1 + \|\dot{\eta}\| + \|\dot{\eta}\|^2$.

Lemma 1 [51]: For $x = [x_1, x_2, \cdots, x_n]^{\mathrm{T}}$, there exists $x^{\mathrm{T}} sign(x) = \sum_{i=1}^{n} |x_i| \geq \|x\|$, i.e., $\|x\|_1 \geq \|x\|$.

Lemma 2 [52]: For a continuously differentiable function $V(x)$ defined in the real domain, let x_0 be the initial value of the variable x, and let c be a positive real number, $0 < \varepsilon < 1$. If the function $V(t)$ satisfies:

$$\dot{V}(x) \leq -cV^{\varepsilon}(x) \tag{12}$$

Then $V(x)$ is finite-time stable, and the settling time T satisfies: $T(x_0) \leq \dfrac{V^{1-\varepsilon}(x_0)}{c(1-\varepsilon)}$.

3. Wave modeling

In many existing studies, environmental disturbances are represented using highly simplified models, which do not fully reflect the underlying physics of wave–structure interactions or the influence of a USV's main dimensions and operational states. Consequently, these simplified descriptions are insufficient for reproducing the complexity of real marine environments. In reality, ocean waves are predominantly short-crested and irregular and exhibit randomness in both frequency and the propagation direction. On the basis of the superposition principle, the resultant wave load is generated not only by components with different frequencies but also by the interaction of wave components traveling in multiple directions. Moreover, wave-induced effects on a USV can be classified into two primary categories. The first-order wave forces mainly induce oscillatory responses in the USV, whereas the second-order components lead to low-frequency drift motions, often termed wave drift forces, which cause gradual deviations in the USV trajectory. To better approximate practical sea conditions, we adopt a short-crested irregular wave model to simulate realistic sea surface wave loads in this work.

First-order wave loads are generally formulated through spectral analysis. In this paper, the ITTC two-parameter wave spectrum is selected to describe the frequency distribution of wave energy. The mathematical expression of the ITTC spectrum is as follows [53]:

$$S_{\zeta}(\omega_{\mathrm{w}}) = \frac{173\overline{H}^2}{T_{\mathrm{p}}^4 \omega_{\mathrm{w}}^5} \exp\left(-\frac{691}{T_{\mathrm{p}}^4 \omega_{\mathrm{w}}^4}\right) \tag{13}$$

where $\overline{H}$ denotes the significant wave height, ω_{w} represents the angular frequency of the waves, and T_{p} represents the wave period, which can be estimated as $T_{\mathrm{p}} = 3.86\sqrt{\overline{H}}$ when the exact period is not available[54].

To account for the angular distribution of wave components traveling in various directions, a directional spreading function is incorporated into the spectral framework, thereby establishing the directional wave spectrum. The associated mathematical expression can be written as follows:

$$S(\omega_{\mathrm{w}}, \theta_{\mathrm{w}}) = S_{\zeta}(\omega_{\mathrm{w}}) \varphi(\theta_{\mathrm{w}}) \tag{14}$$

where $S(\omega_{\mathrm{w}}, \theta_{\mathrm{w}})$ denotes the wave spectrum, and $\varphi(\theta_{\mathrm{w}})$ represents the spreading function, with $\varphi(\theta_{\mathrm{w}}) = \dfrac{2}{\pi} \cos^2(\theta_{\mathrm{w}})$.

The encounter angle between the USV's heading and the component wave propagating in the j-th direction is defined as $\chi_j = \psi - \theta_{\mathrm{w}j}$. For incident waves with the i-th frequency, the corresponding encounter frequency experienced by the USV can be expressed as $\omega_{\mathrm{we}i} = \omega_{\mathrm{w}i} - Vk_i \cos\chi_j = \omega_{\mathrm{w}i} - \omega_{\mathrm{w}i}^2 \cdot V \cos\chi_j / g$.

The first-order wave force is given by the following expression:

$$X = \sum_{i=1}^{n}\sum_{j=1}^{m} \frac{-2\rho g B \zeta_{A_{ij}}}{k_i F_{ij}} \cdot \sin E_{ij} \cdot C_i \sin F_{ij} \cdot \sin\left(\omega_{\mathrm{we}i} t - \varepsilon_{ij}\right) \tag{15}$$

$$Y = \sum_{i=1}^{n}\sum_{j=1}^{m} \frac{2\rho g L \zeta_{A_{ij}}}{k_i E_{ij}} C_i \sin E_{ij} \sin F_{ij} \sin\left(\omega_{\mathrm{we}i} t - \varepsilon_{ij}\right) \tag{16}$$

$$N = \sum_{i=1}^{n}\sum_{j=1}^{m} -\frac{\rho g L^2 B \zeta_{A_{ij}}}{E_{ij} F_{ij}} C_i \sin F_{ij} \cos\left(\omega_{\mathrm{we}i} t - \varepsilon_{ij}\right)\left(\frac{\sin E_{ij}}{E_{ij}} - \cos E_{ij}\right) \tag{17}$$

where $\zeta_{A_{cij}} = \sqrt{2S\left(\omega_{\mathrm{w}i}, \theta_{\mathrm{w}j}\right)\Delta\omega_{\mathrm{w}}\Delta\theta_{\mathrm{w}}}$, $C_i = 1 - e^{-k_i d_{\mathrm{s}}}$, $E_{ij} = \frac{k_i L \cos\chi_j}{2}$, $F_{ij} = \frac{k_i B \sin\chi_j}{2}$, $k_i = \omega_{\mathrm{w}i}^2 / g$, L denotes the ship length, B denotes the ship breadth, and d_{s} denotes the draft, $\Delta\omega_{\mathrm{w}}$ represents the frequency interval, and $\Delta\theta_{\mathrm{w}}$ denotes the directional interval of wave incidence.

Remark 1. In many numerical implementations, the representative frequency of each discretized spectral band is taken directly as the upper (or lower) boundary of that band. Such a deterministic selection may introduce artificial periodic patterns into the simulated wave field. To mitigate this effect, in the present study, the whole frequency range is first uniformly divided into 50 sub-intervals. Then, one frequency is randomly selected from each sub-interval and taken as the representative frequency of the corresponding component wave. In this way, the full frequency domain is effectively spanned while spurious periodicity in the time-domain response is reduced, leading to a more faithful reproduction of the random characteristics of ocean waves.

The second-order wave drift force influences both a USV's heading and its overall trajectory. Although its rigorous theoretical derivation is mathematically involved, this force is generally considered to be proportional to the square of the wave amplitude. Therefore, the wave drift force can be formulated in the following general form:

$$X_D = \sum_{i=1}^{n}\sum_{j=1}^{m} \frac{1}{2}\rho g L \zeta_{A_{ij}}^2 \cos\chi_j C_{X_{\mathrm{w}Di}}\left(\frac{\lambda_i}{L}\right) \tag{18}$$

$$Y_D = \sum_{i=1}^{n}\sum_{j=1}^{m} \frac{1}{2}\rho g L \zeta_{A_{ij}}^2 \sin\chi_j C_{Y_{\mathrm{w}Di}}\left(\frac{\lambda_i}{L}\right) \tag{19}$$

$$N_D = \sum_{i=1}^{n}\sum_{j=1}^{m} \frac{1}{2}\rho g L^2 \zeta_{A_{ij}}^2 \sin\chi_j C_{N_{\mathrm{w}Di}}\left(\frac{\lambda_i}{L}\right) \tag{20}$$

where $C_{X_{\mathrm{w}Di}}$, $C_{Y_{\mathrm{w}Di}}$, and $C_{N_{\mathrm{w}Di}}$ denote the coefficients determined by the ratio between the incident wavelength and the ship length. Their specific formulations are given as follows:

$$C_{X_{\mathrm{w}Di}} = 0.05 - 0.2\left(\frac{\lambda_i}{L}\right) + 0.75\left(\frac{\lambda_i}{L}\right)^2 - 0.51\left(\frac{\lambda_i}{L}\right)^3 \tag{21}$$

$$C_{Y_{\mathrm{w}Di}} = 0.46 + 6.83\left(\frac{\lambda_i}{L}\right) - 15.65\left(\frac{\lambda_i}{L}\right)^2 + 8.44\left(\frac{\lambda_i}{L}\right)^3 \tag{22}$$

$$C_{N_{\mathrm{w}Di}} = -0.11 + 0.68\left(\frac{\lambda_i}{L}\right) - 0.79\left(\frac{\lambda_i}{L}\right)^2 + 0.21\left(\frac{\lambda_i}{L}\right)^3 \tag{23}$$

The main wave direction is set to 90°, and the directional coverage interval is taken as 25°–155°. The number of frequency discretization intervals is 50, and the number of directional component waves is also 50.

To determine the representative component frequencies, the whole frequency range is first uniformly divided into 50 sub-intervals, and then one frequency is randomly selected from each sub-interval. In this way, the full frequency range is covered while the artificial periodicity caused by fixed endpoint selection can be reduced. The relevant parameter settings in the simulations of this paper are as follows: $\overline{H}=0.02$, $T_p=0.55$, $L=1.225$, $B=0.29$, $d_s=0.12$, $\Delta\omega_w=7\pi/25$, $\Delta\theta_w=13\pi/900$, $\theta_w\in[5\pi/36,31\pi/36]$, $\omega_w\in[0,14\pi]$, $g=9.8$.

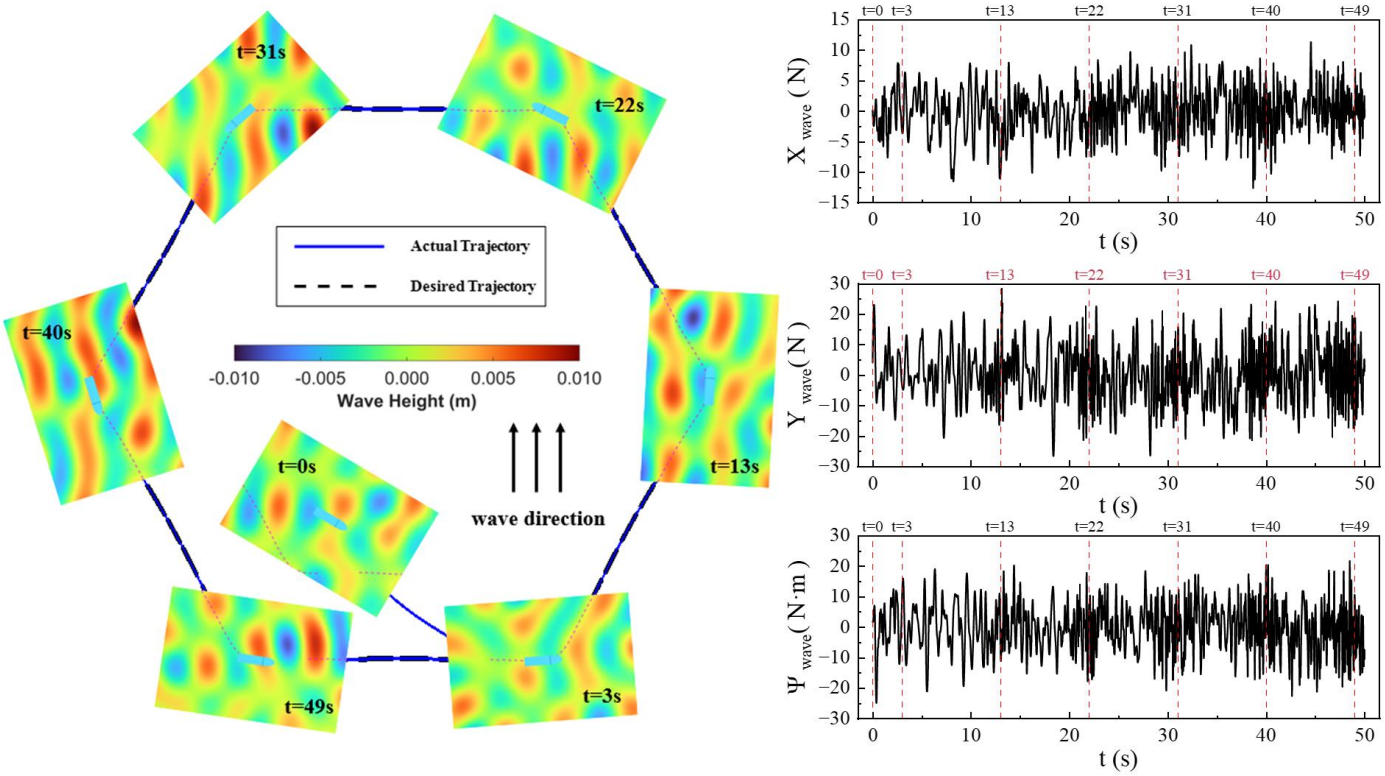

Fig. 2 Relationship between short-crested wave fields and wave forces acting on a USV during trajectory tracking

The representative wave forces generated by the proposed short-crested wave model and the corresponding USV trajectory tracking under wave disturbances are shown in Figure 2. Here, X_{wave}, Y_{wave}, and ψ_{wave} denote the wave-induced surge force, sway force, and yaw moment, respectively, each representing the result of the first- and second-order wave forces in the corresponding degree of freedom. As shown in the figure, during the trajectory tracking process in short-crested waves, the wave forces acting on a USV vary over time, as reflected by the time histories on the right, which correspond to the short-crested wave fields encountered along the trajectory illustrated on the left.

4. Controller design

In this section, the mathematical model of the controller and its stability analysis are presented. First, in Section 4.1, a predefined time nonsingular terminal sliding mode controller is designed by addressing the limitations of traditional nonsingular terminal sliding mode control and incorporating predefined time control methods. In Section 4.2, the case of unknown disturbance upper bounds is further considered, leading to the design of a predefined time adaptive nonsingular terminal sliding mode controller. The structure of the predefined time adaptive nonsingular terminal sliding mode controller is shown in Figure 3.

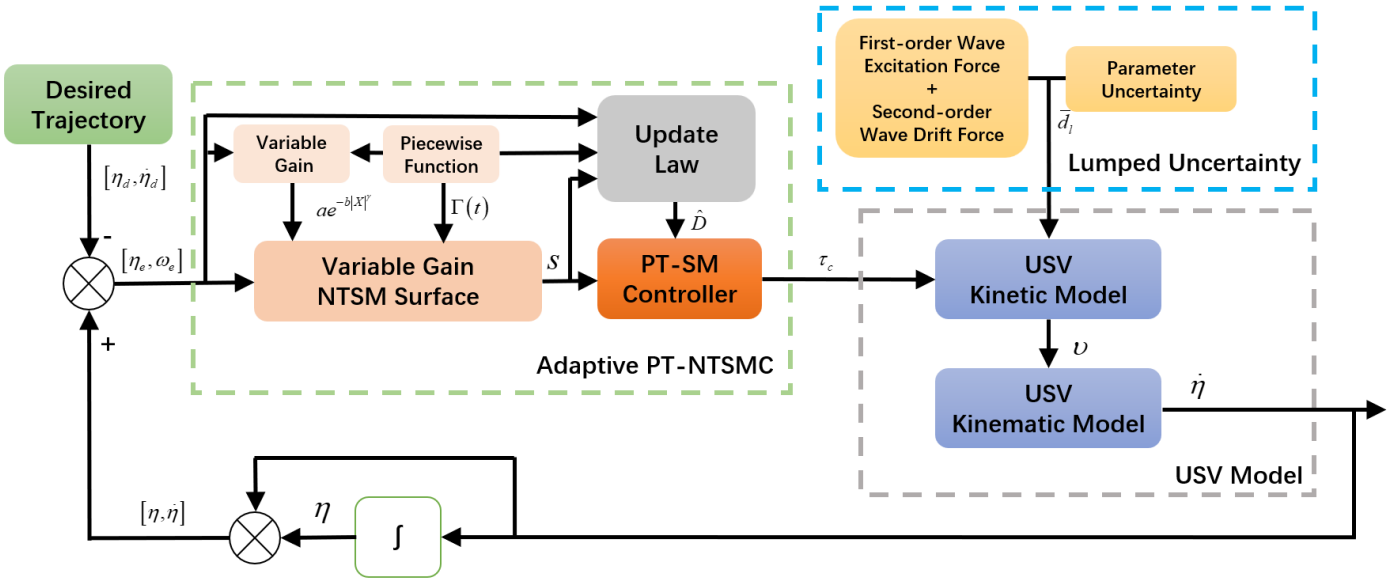

Fig. 3 Structure of the adaptive PT-NTSMC

4.1 Design of the predefined time nonsingular terminal sliding mode controller

Remark 2: The structure of the traditional nonsingular terminal sliding mode control can be expressed as [55] :

$$\sigma = x + \beta \mathrm{sig}^{\mu}(\dot{x}) = 0, \quad \beta > 0, \quad 1 < \mu < 2 \tag{24}$$

According to Equation (24), although the traditional nonsingular terminal sliding mode control has a simple structure, it has the following limitations:

(1) The parameter β is proportional to the system's convergence speed. A relatively large value is usually required at the initial stage to accelerate error convergence, but this inevitably increases the control input.

(2) The convergence time cannot be specified explicitly in advance.

To overcome the above limitations, a variable-gain sliding mode manifold is constructed as follows:

$$s = a\mathrm{e}^{-b|X|^{\gamma}} \circ X + \mathrm{sig}^{\alpha}(\dot{X}) \tag{25}$$

where $X = \eta_e - \Gamma(t)$, $\dot{X} = \omega_e - \dot{\Gamma}(t)$, $a = \mathrm{diag}(a_1, a_2, a_3)$ $a_i > 0$, $\gamma = (\alpha - 1)/\alpha, 1 < \alpha < 2$, b is a positive constant. To overcome the limitation of the conventional fixed-gain design, $ae^{-b|X|^{\gamma}}$ is introduced as the gain coefficient in Equation (25). Because X varies during the control process, this coefficient changes accordingly and thus constitutes a variable-gain term. In particular, as $|X|$ decreases, thereby accelerating the error convergence and enabling a relatively small gain coefficient to achieve a fast convergence rate. It can be observed that when $b = 0$ or $X = 0_{3\times1}$, Equation (25) is transformed into:

$$s = aX + \mathrm{sig}^{\alpha}(\dot{X}) \tag{26}$$

$\Gamma(t)$ is a piecewise function that is continuous and twice differentiable within $t \in [0, +\infty)$.

$$\Gamma(t) = \begin{cases} (T-t)^{\delta} \mathrm{e}^{\kappa/(t-T)} \chi & 0 \le t < T \\ 0_{3\times1} & T \le t \end{cases} \tag{27}$$

where $\chi = [\chi_1, \chi_2, \chi_3]^{\mathrm{T}}$ is an undetermined parameter vector, $\delta > 4$, κ is a positive constant, and T is the predefined time parameter. The time-varying function $\Gamma(t)$ should satisfy the following conditions:

$$s(0)=a\mathrm{e}^{-b|X(0)|^{\gamma}}\circ X(0)+\mathrm{sig}^{\alpha}\left(\dot{X}(0)\right)=0 \tag{28}$$

Taking the derivative of Equation (25) yields:

$$\dot{s}=a\mathrm{e}^{-b|X(t)|^{\gamma}}\circ\dot{X}(t)\circ\left(I_{3\times1}-b\gamma\left|X(t)\right|^{\gamma}\right)+\alpha\left|\dot{X}(t)\right|^{\alpha-1}\circ\ddot{X}(t) \tag{29}$$

The predefined time control law is designed as:

$$\tau_c(t)=\tau_{eq}(t)+\tau_{sw}(t) \tag{30}$$

The predefined-time control law is composed of two parts: the equivalent control term τ_{eq} and the switching control term τ_{sw}, whose expressions are given in Equations (31) and (32), respectively. Specifically, τ_{eq} is derived by substituting the nominal system dynamics into Equation (31) and imposing $\dot{s}=0$, and is used to compensate for the nominal system dynamics and preserve the desired sliding motion on the manifold. Meanwhile, τ_{sw} is designed to suppress lumped disturbances and model uncertainties, thereby ensuring the reachability and robustness of the sliding mode.

$$\tau_{eq}(t)=R^{-1}(\psi)\left\{\begin{array}{l}\bar{M}_n(\eta)\left[\begin{array}{l}-\dfrac{a}{\alpha}e^{-b|X(t)|^{\gamma}}\circ\left(I_{3\times1}-b\gamma\left|X(t)\right|^{\gamma}\right)\circ sig^{2-\alpha}\left(\dot{X}(t)\right)\\+\ddot{\Gamma}(t)+\ddot{\eta}_d\end{array}\right]\\+\bar{C}_n(\upsilon,\eta)\dot{\eta}+\bar{D}_n(\upsilon,\eta)\dot{\eta}\end{array}\right\} \tag{31}$$

$$\tau_{sw}(t)=-R^{-1}(\psi)\bar{M}_n(\eta)\left(D_1+\rho\right)sign(s) \tag{32}$$

where ρ is a positive minimal value, $D_1=\left\|\bar{M}_n^{-1}(\eta)\right\|D_l$.

Theorem 1: If the sliding mode manifold is designed according to Eq. (26) and (27), and the controller is designed according to Equations (30) – (32), then the sliding variable satisfies $s(t)=0,\ \forall t\in[0,+\infty)$.

Therefore, the closed-loop system achieves global sliding mode.

Proof: Let the Lyapunov function be chosen as:

$$V_1=\frac{1}{2}s^{\mathrm{T}}s \tag{33}$$

Taking the time derivative of Equation (33) gives $\dot{V}_1=s^{\mathrm{T}}\dot{s}$, and expanding it using Equation (28) results in:

$$\dot{V}_1=s^{\mathrm{T}}\left[a\cdot\mathrm{e}^{-b|X(t)|^{\gamma}}\circ\dot{X}(t)\circ\left(I_{3\times1}-b\gamma\left|X(t)\right|^{\gamma}\right)+\alpha\left|\dot{X}(t)\right|^{\alpha-1}\circ\ddot{X}(t)\right] \tag{34}$$

By further computing Equation (34) using Equations (8), (30), (31), and (32), the following result is obtained:

$$\begin{aligned}\dot{V}_1&=s^{\mathrm{T}}\left[\alpha\left|\dot{X}(t)\right|^{\alpha-1}\circ\left(\bar{M}_n^{-1}(\eta)\bar{d}_l(t,\upsilon,\eta)-\left(D_1+\rho\right)\mathrm{sign}(s)\right)\right]\\&\le\alpha\left\|s^{\mathrm{T}}\left|\dot{X}(t)\right|^{\alpha-1}\right\|\left(\left\|\bar{M}_n^{-1}(\eta)\bar{d}_l(t,\upsilon,\eta)\right\|-\left(D_1+\rho\right)\right)\end{aligned} \tag{35}$$

According to **Lemma 1** and **Assumption 2**, it follows that:

$$\begin{aligned}\dot{V}_1 &\le \alpha \left\| s^{\mathrm{T}} \left| \dot{X}(t) \right|^{\alpha-1} \right\|_1 \left(\left\| \bar{d}_l(t,\upsilon,\eta) \right\| - (D_1+\rho) \right) \\ &\le \alpha\lambda \left\| s^{\mathrm{T}} \left| \dot{X}(t) \right|^{\alpha-1} \right\|_1 \left(\left\| \bar{d}_l(t,\upsilon,\eta) \right\| - \left(l_0 + l_1 \|\dot{\eta}\| + l_2 \|\dot{\eta}\|^2 + \rho' \right) \right) \le 0 \end{aligned} \tag{36}$$

where $\rho' = \rho/\lambda$, λ represents the upper bound of $\left\| \bar{M}_n^{-1}(\eta) \right\|$. Since ρ is a positive minimal value, it can be considered as $\rho' = \rho$.

The piecewise function $\Gamma(t)$ designed in this paper ensures that Equation (28) holds, thus for Equation (33), $V_1(0) = \frac{1}{2} s(0)^{\mathrm{T}} s(0) = 0$ and $V_1(t) \ge 0,\ \forall t \in [0,+\infty)$. Moreover, according to Inequality (34), it follows that $V_1(t) \le V_1(0),\ \forall t \in (0,+\infty)$. Consequently, the conclusion is obtained: $V_1(t) = 0,\ \forall t \in [0,+\infty)$. That is, $s(t) = 0,\ \forall t \in [0,+\infty)$. Thus, the closed-loop system achieves the global sliding-mode property, and Theorem 1 is proved.

Based on the conclusion of **Theorem 1** and Equation (25), we have:

$$\dot{X}(t) = -a^{\frac{1}{\alpha}} \mathrm{e}^{-\frac{b}{\alpha}|X(t)|^{\gamma}} \circ \mathrm{sig}^{\frac{1}{\alpha}}\left(X(t) \right) \tag{37}$$

Theorem 2. If the variable-gain sliding mode manifold in Equation (25) satisfies **Theorem 1**, then the position tracking error η_e converges to the origin in finite time.

Proof. For the *i*-th DOF, consider the following Lyapunov function:

$$V_{2i} = \frac{1}{2} X_i^2(t), \quad i = 1,2,3. \tag{38}$$

Taking the time derivative of V_{2i} yields:

$$\dot{V}_{2i} = X_i(t) \dot{X}_i(t) \tag{39}$$

Substituting Equation (37) into Equation (39) gives:

$$\begin{aligned}\dot{V}_{2i} &= X_i(t) \left(-a^{\frac{1}{\alpha}} \mathrm{e}^{-\frac{b}{\alpha}|X_i(t)|^{\gamma}} \mathrm{sig}^{\frac{1}{\alpha}}\left(X_i(t) \right) \right) \\ &= -a^{\frac{1}{\alpha}} \mathrm{e}^{-\frac{b}{\alpha}|X_i(t)|^{\gamma}} \left| X_i(t) \right|^{1+\frac{1}{\alpha}} \\ &= -A \mathrm{e}^{-B V_{2i}^{\gamma/2}} V_{2i}^{(\alpha+1)/(2\alpha)} \end{aligned} \tag{40}$$

where $A = 2^{(\alpha+1)/(2\alpha)} a^{1/\alpha}$, $B = \frac{2^{\gamma/2} b}{\alpha}$. Solving the differential equation in Equation (40), the time for V_{2i} to converge to zero is $T_{0i} = \frac{\alpha \left(\mathrm{e}^{\frac{b}{\alpha}|X_i(0)|^{\gamma}} - 1 \right)}{b\gamma a^{1/\alpha}}$, $i = 1,2,3$, $T_0 = \left[T_{01}, T_{02}, T_{03} \right]^{\mathrm{T}}$. From the above conclusion, it is known that $X_i(t)$ converges to zero at time T_{0i}. Typically, the values of T_{0i} are chosen to be the same. Furthermore, according to Equation (27), the piecewise function $\Gamma(t)$ satisfies $\Gamma(t) = 0,\ \forall t \ge 0$, which implies that the time at which the position error η_e converges to zero can be expressed as $T_c = \max(T_0, T)$. This means that the following relationship holds between η_e and $\Gamma(t)$:

1) When $T \le T_0$:

$$\begin{cases} \eta_e \neq 0, \Gamma(t) \neq 0 & 0 \le t < T \\ \eta_e \neq 0, \Gamma(t) = 0 & T \le t < T_0 \\ \eta_e = 0, \Gamma(t) = 0 & T_0 \le t \end{cases}$$

2) When $T_0 < T$:

$$\begin{cases} \eta_e \neq 0, \Gamma(t) \neq 0 & 0 \le t < T_0 \\ \eta_e = 0, \Gamma(t) \neq 0 & T_0 \le t < T \\ \eta_e = 0, \Gamma(t) = 0 & T \le t \end{cases}$$

Remark 3. At this stage, the undetermined parameter vector χ in the piecewise function $\Gamma(t)$ and the gain term a in the sliding mode manifold need to be specified. On the basis of the conclusion in **Theorem 2**, without loss of generality, let $T \le T_0$, which leads to $T_c = T_0$. Then, by substituting the initial conditions of the sliding mode function in Equation (26), both χ and a can be determined from the system of equations given in Equation (41).

$$\begin{cases} T_c = \dfrac{\alpha\left(\mathrm{e}^{\frac{b}{\alpha}|X(0)|^{\gamma}} - 1\right)}{b\gamma a^{1/\alpha}} \\ a\mathrm{e}^{-b|X(0)|^{\gamma}} \circ X(0) + \mathrm{sig}^{\alpha}\left(\dot{X}(0)\right) = 0 \end{cases} \tag{41}$$

where $\Gamma(0) = T^{\delta}\mathrm{e}^{-\kappa/T}\chi$, $\dot{\Gamma}(0) = -T^{\delta-1}\mathrm{e}^{-\kappa/T}\chi\left(\delta + \dfrac{\kappa}{T}\right)$.

Remark 4. The parameters that need to be specified manually in the controller mainly include T, T_c, κ, δ, b and α. The value of T directly affects the convergence speed of the tracking error. Although T can theoretically be any positive number, a smaller T requires greater control effort. Therefore, in practice, T should be selected considering both the performance limits of the USV and the magnitude of the initial tracking error. The parameter T_c (or T_0) denotes the time when the sum of the tracking error and the time-varying function converges to zero, and it is usually chosen to be equal to T in practical implementation. The constant κ affects the rate of variation of the time-varying function, but it has little influence on the overall control performance. The parameter δ must be greater than 4 to ensure that the derivative of the time-varying function exhibits characteristics similar to the function itself over the entire time domain. The value of b determines the variation rate of the gain term. A larger b makes the gain coefficient change more rapidly with the tracking error, thereby making the variable-gain effect more pronounced. Consequently, b influences the trade-off between convergence speed and control amplitude in the proposed controller. Finally, α influences the nonlinearity of the sliding manifold. A larger α enhances convergence in the large-error region but may produce excessive control effort and induce chattering near equilibrium. Conversely, a smaller α yields smoother control with reduced chattering, albeit at the cost of a slightly slower convergence rate.

4.2 Design of the adaptive predefined time nonsingular terminal sliding mode controller

In Equations (30), (31), and (32) of Section 4.1, the mathematical model of the predefined time controller is given. According to Assumption 1, in the switching control law given in Equation (32), to enable the controller to counteract the effect of lumped uncertainties, the upper bound of the lumped disturbance needs to be provided. This ensures that the controlled state can slide along the sliding mode surface to the origin after it is reached. However, in practical situations, the upper bound of lumped disturbances is often difficult to obtain and is typically given in constant form. If the given value is too small, the effective suppression of

the lumped disturbance by the controller cannot be ensured. On the other hand, if the given value is too large, it can lead to overly aggressive control actions and unnecessarily large control amplitudes, which may increase actuator burden and potentially damage the USV actuators.

To address these issues, an adaptive predefined time control law is proposed in this section. By estimating the upper bound of the lumped disturbance using the system states, the proposed method confines the disturbance-bound-related parameter dependence to the interval before the predefined time, rather than the entire control process as in many existing methods.

According to Equation (32), let $\hat{D}_1$ represent the estimated value of the lumped disturbance upper bound. Then, $\hat{D}_1$ can be expressed as:

$$\hat{D}_1 = \left\| \bar{M}_n^{-1}(\eta) \right\| \hat{l} \mathrm{H} \tag{42}$$

where $\hat{l}$ is the estimated value of l, and $\Delta l = \hat{l} - l$ represents the estimation error. The update law for the parameter l is as follows:

$$\dot{\hat{l}} = \varsigma \left\| \bar{M}_n^{-1}(\eta) \right\| \left\| s^{\mathrm{T}} \right\| \left| \dot{X}(t) \right|^{\alpha-1} \mathrm{H} \tag{43}$$

where ς is a positive constant. The mathematical model of the predefined time adaptive controller is designed as:

$$\begin{aligned} \hat{\tau}_c(t) &= \tau_{eq}(t) + \hat{\tau}_{sw}(t) \\ &= R^{-1}(\psi) \left\{ \begin{bmatrix} \bar{M}_n(\eta) \begin{bmatrix} -\dfrac{a}{\alpha} e^{-b\left|X(t)\right|^{\gamma}} \circ \left(I_{3\times 1} - b\gamma \left| X(t) \right|^{\gamma} \right) \circ sig^{2-\alpha}\left(\dot{X}(t) \right) \\ +\ddot{\Gamma}(t) + \ddot{\eta}_d \end{bmatrix} \\ +\bar{C}_n(\upsilon,\eta)\dot{\eta} + \bar{D}_n(\upsilon,\eta)\dot{\eta} \end{bmatrix} \right\} \\ &\quad -R^{-1}(\psi)\bar{M}_n(\eta)\left[L_0 s + \left(\hat{D}_1 + \rho \right) \mathrm{sign}(s) \right] \end{aligned} \tag{44}$$

where L_0 should be chosen as a value greater than the upper bound of the disturbance. At the initial moment, when $\hat{D}_1$ is relatively small, the term L_0 contributes primarily to disturbance suppression. As time progresses and $\hat{D}_1$ approaches the upper bound of the disturbance at the predefined time, s decreases, and the second term then plays the dominant role in suppressing the disturbance. To avoid the chattering phenomenon caused by the sign function, the saturation function is used instead, as detailed in **Remark 3**.

Theorem 3. For the USV motion model given in Equation (1) and **Assumptions 1-2**, if the sliding mode manifold has the form of Equation (25), the adaptive controller has the form of Equation (44), and the adaptive update law has the form of Equation (43); then, the position errors η_e and Δl converge to zero within finite time.

Proof. The Lyapunov function is established as follows:

$$V_3 = \frac{1}{2} s^{\mathrm{T}} s + \frac{\alpha l}{2} \left(\hat{l} - l \right)^2 \tag{45}$$

Taking the time derivative of Equation (45) yields:

$$\begin{aligned} \dot{V}_3 &= s^{\mathrm{T}} \dot{s} + \alpha l \left(\hat{l} - l \right) \dot{\hat{l}} \\ &= s^{\mathrm{T}} \left[\alpha \left| \dot{X}(t) \right|^{\alpha-1} \circ \left(\bar{M}_n^{-1}(\eta) \bar{d}_l(t,\upsilon,\eta) - L_0 s - \left(\hat{D}_1 + \rho \right) \mathrm{sign}(s) \right) \right] \\ &\quad +\alpha l \varsigma \left(\hat{l} - l \right) \left\| \bar{M}_n^{-1}(\eta) \right\| \left\| s^{\mathrm{T}} \right\| \left| \dot{X}(t) \right|^{\alpha-1} \mathrm{H} \end{aligned} \tag{46}$$

By substituting Equation (42) into Equation (46), we obtain:

$$\begin{aligned}\dot{V}_3 &= s^{\mathrm{T}}\dot{s}+\alpha l\left(\hat{l}-l\right)\dot{\hat{l}}\\ &= s^{\mathrm{T}}\left[\alpha\left|\dot{X}(t)\right|^{\alpha-1}\circ\begin{pmatrix}\bar{M}_n^{-1}(\eta)\bar{d}_l(t,\upsilon,\eta)-L_0 s-\rho\,\mathrm{sign}(s)\\ -\left\|\bar{M}_n^{-1}(\eta)\right\|\hat{l}\,\mathrm{H}\,\mathrm{sign}(s)\end{pmatrix}\right]\\ &+\alpha l\varsigma\left(\hat{l}-l\right)\left\|\bar{M}_n^{-1}(\eta)\right\|\left|s^{\mathrm{T}}\right|\left|\dot{X}(t)\right|^{\alpha-1}\mathrm{H}\\ &= \alpha\left(\left|\dot{X}(t)\right|^{\alpha-1}\right)^{\mathrm{T}}\begin{bmatrix}\bar{M}_n^{-1}(\eta)\bar{d}_l(t,\upsilon,\eta)\circ s-L_0 s\circ s-\rho|s|\\ -\left\|\bar{M}_n^{-1}(\eta)\right\|\hat{l}\,\mathrm{H}|s|\end{bmatrix}\\ &+\alpha l\varsigma\left(\hat{l}-l\right)\left\|\bar{M}_n^{-1}(\eta)\right\|\left(\left|\dot{X}(t)\right|^{\alpha-1}\right)^{\mathrm{T}}|s|\mathrm{H}\\ &+\alpha\left(\left|\dot{X}(t)\right|^{\alpha-1}\right)^{\mathrm{T}}\left\|\bar{M}_n^{-1}(\eta)\right\|l\mathrm{H}|s|-\alpha\left(\left|\dot{X}(t)\right|^{\alpha-1}\right)^{\mathrm{T}}\left\|\bar{M}_n^{-1}(\eta)\right\|l\mathrm{H}|s|\end{aligned}\tag{47}$$

From Equation (47), one can derive

$$\begin{aligned}\dot{V}_3 &= \alpha\left(\left|\dot{X}(t)\right|^{\alpha-1}\right)^{\mathrm{T}}\begin{bmatrix}\bar{M}_n^{-1}(\eta)\bar{d}_l(t,\upsilon,\eta)\circ s-L_0 s^2-\rho|s|\\ -\left\|\bar{M}_n^{-1}(\eta)\right\|l\mathrm{H}|s|\end{bmatrix}\\ &+\alpha l\varsigma\Delta l\left\|\bar{M}_n^{-1}(\eta)\right\|\left(\left|\dot{X}(t)\right|^{\alpha-1}\right)^{\mathrm{T}}|s|\mathrm{H}\\ &-\alpha\left(\left|\dot{X}(t)\right|^{\alpha-1}\right)^{\mathrm{T}}\left\|\bar{M}_n^{-1}(\eta)\right\|\Delta l\mathrm{H}|s|\\ &= \alpha\left(\left|\dot{X}(t)\right|^{\alpha-1}\right)^{\mathrm{T}}\begin{bmatrix}\bar{M}_n^{-1}(\eta)\bar{d}_l(t,\upsilon,\eta)\circ s-L_0 s^2-\rho|s|\\ -\left\|\bar{M}_n^{-1}(\eta)\right\|l\mathrm{H}|s|\end{bmatrix}\\ &-\alpha(1-l\varsigma)\left(\left|\dot{X}(t)\right|^{\alpha-1}\right)^{T}\left\|\bar{M}_n^{-1}(\eta)\right\|\Delta l\mathrm{H}|s|\end{aligned}\tag{48}$$

Choose an appropriate parameter ς such that $0<\varsigma l<1$, then the following inequality holds:

$$\begin{aligned}\dot{V}_3 &\le \alpha\left(\left|\dot{X}(t)\right|^{\alpha-1}\right)^{\mathrm{T}}\left(\left\|\bar{M}_n^{-1}(\eta)\bar{d}_l(t,\upsilon,\eta)\right\|-\rho-\left\|\bar{M}_n^{-1}(\eta)\right\|l\mathrm{H}\right)|s|\\ &-\alpha(1-l\varsigma)\left(\left|\dot{X}(t)\right|^{\alpha-1}\right)^{\mathrm{T}}\left\|\bar{M}_n^{-1}(\eta)\right\|\left|\Delta l\right|\mathrm{H}|s|\end{aligned}\tag{49}$$

Let

$$\begin{aligned}\Theta &= -\alpha\left(\left|\dot{X}(t)\right|^{\alpha-1}\right)^{\mathrm{T}}\left(\left\|\bar{M}_n^{-1}(\eta)\bar{d}_l(t,\upsilon,\eta)\right\|-\rho-\left\|\bar{M}_n^{-1}(\eta)\right\|l\mathrm{H}\right)\\ \Lambda &= \alpha(1-l\varsigma)\left(\left|\dot{X}(t)\right|^{\alpha-1}\right)^{\mathrm{T}}|s|\left\|\bar{M}_n^{-1}(\eta)\right\|\mathrm{H}\end{aligned}\tag{50}$$

Then, Inequality (49) can be equivalently rewritten as:

$$\dot{V}_3 \le -\Theta|s|-\Lambda|\Delta l|\tag{51}$$

From Equation (50), it follows that $\Theta \geq 0_{1\times 3}$, $\Lambda \geq 0$. Inequality (51) is rewritten and further relaxed as:

$$\begin{aligned}\dot{V}_3 &\leq -\sum_{i=1}^{3}\sqrt{2}\Theta_i\frac{|s_i|}{\sqrt{2}}-\frac{\sqrt{2}}{\sqrt{\alpha l}}\Lambda\frac{\sqrt{\alpha l}}{\sqrt{2}}|\Delta l| \\ &\leq -\Upsilon\left(\sum_{i=1}^{3}\frac{|s_i|}{\sqrt{2}}+\frac{\sqrt{\alpha l}}{\sqrt{2}}|\Delta l|\right) \\ &\leq -\Upsilon\sqrt{\sum_{i=1}^{3}\frac{s_i^2}{\sqrt{2}}+\frac{\alpha l}{2}(\Delta l)^2} \\ &= -\Upsilon V_3^{1/2}\end{aligned} \tag{52}$$

where $\Upsilon=\min\left(\sqrt{2}\Theta_1,\sqrt{2}\Theta_2,\sqrt{2}\Theta_3,\frac{\sqrt{2}}{\sqrt{\alpha l}}\Lambda\right)$. According to **Lemma 2**, V_3 converges to zero within a finite time. The convergence time satisfies $T_1 \leq \frac{2V^{1/2}(0)}{\Upsilon}$. This conclusion is equivalent to stating that the combination of s and Δl converges to zero within the finite time T_1 . Since Δl converges to zero, $\hat{D}_1$ becomes sufficiently large to enable the switching control term to effectively suppress external disturbances. Therefore, analogous to the proof process of **Theorem 2**, it can be concluded that η_e will also converge to zero within a finite time.

Remark 5. The respective roles of the three components in the proposed method are different. The predefined time sliding mode manifold and controller structure are responsible for establishing a predefined upper bound on the convergence time. The global sliding mode construction removes the reaching phase and enhances robustness from the initial instant. The adaptive law is introduced to estimate the unknown disturbance bound online, thereby improving practicality and reducing conservativeness in controller design.

Remark 6. Notably, the sign function is adopted in the switching control term for disturbance rejection. Nevertheless, due to the discontinuous nature of the sign function at zero crossing, together with the fact that the coefficients preceding the sign function in Equations (32) and (44) remain nonzero as the sliding mode variable approaches zero, abrupt changes in the switching control input occur when the sign of the sliding variable reverses. This inevitably gives rise to chattering. In engineering applications, chattering may lead to increased actuator wear, material fatigue, and reduced operational efficiency. Therefore, a saturation function is introduced in place of the sign function in the present study to suppress chattering.

$$f_{sat}(x)=\begin{cases} x/h, & |x|\leq h \\ \operatorname{sign}(x), & |x|>h \end{cases} \tag{53}$$

where $h>0$.

5. Simulation results and analysis

In this chapter, a simulation-based comparative analysis is conducted to verify the control performance of the predefined time controllers proposed in Sections 4.1 and 4.2. The ship parameters used in the simulation are based on Cybership II from the Norwegian University of Science and Technology (NTNU) [56]. As this model has been widely used in USV performance simulations, its adoption in this study enhances the generality of comparative results.

In Section 5.1, the initial position of the USV is set to $\eta_0=[-1,-2,-\pi/6]^{\mathrm{T}}$, and the initial velocity is set to $\upsilon_0=[0,0,0]^{\mathrm{T}}$ for the simulation. The disturbance adopted in Section 5.1 is given as follows:

$$d=\begin{bmatrix} 10\sin\left(0.04t\right) \\ 10\left(1-\cos\left(0.04t\right)\right) \\ 0.04t \end{bmatrix} \tag{54}$$

In Section 5.2, the initial state of the USV is provided. The external unknown disturbance acting on the USV is modeled using the short-crested irregular wave force model introduced in Section 3. In all comparative simulation cases, the same wave parameters, including the randomly generated frequencies, propagation directions, and initial phases, are used in the wave force model to ensure a fair comparison among different controllers. The given target trajectory is as follows:

$$\eta_d=\begin{bmatrix} x_d \\ y_d \\ \psi_d \end{bmatrix}=\begin{bmatrix} 0.2\left(20\sin\left(6t/50\right)+1.2\sin\left(30t/50\right)\right) \\ 0.2\left(-20\cos\left(6t/50\right)+1.2\cos\left(30t/50\right)\right) \\ \arctan\left(\dot{y}_d/\dot{x}_d\right) \end{bmatrix} \tag{55}$$

The relevant coefficients in the inertia matrix vary because of changes in the USV load. Therefore, it is necessary to consider the impact of system parameter variations on the controller's performance. In accordance with the definition given in Section 2.1, $\Delta*$ represents the uncertainty coefficients in the parameter error matrix $*_u$, and we assume that the parameter variations follow the patterns given below:

$$\begin{aligned} &\Delta m_{11}=0.2m'_{11}\sin(0.1t); && \Delta m_{22}=0.2m'_{22}\sin(0.2t+\pi/4); \\ &\Delta m_{23}=0.2m'_{23}\sin(0.1t+\pi/3); && \Delta m_{33}=0.2m'_{33}\sin(0.1t+\pi/6); \\ &\Delta d_{11}=0.2d'_{11}\sin(0.1t+\pi/3); && \Delta d_{22}=0.2d'_{22}\sin(0.2t+\pi/2); \\ &\Delta d_{23}=0.2d'_{23}\sin(0.2t); && \Delta d_{32}=0.2d'_{32}\sin(0.2t+\pi/6). \end{aligned} \tag{56}$$

5.1 Control performance of the predefined time nonsingular terminal sliding mode controller

In this section, trajectory tracking simulations are carried out in the MATLAB R2024a environment to validate the effectiveness of the proposed controller. The predefined time controller designed in Section 4.1 is validated through simulation. First, the existing SMC methods are applied to the same scenario, and a comparative analysis is conducted to validate the performance of the proposed controller. Second, simulations are performed under five different initial conditions to verify the controller's performance under various operating scenarios. Finally, simulations are carried out under different predefined time requirements to validate the controller's predefined time convergence performance under various time constraints.

First, the fast terminal sliding mode control (FTSMC) method and the adaptive integral fast terminal sliding mode control (AI-FTSMC) method, as presented in reference [57], are selected for comparison. The sliding mode manifolds for both methods are as follows:

$$s=\omega_e+\int_0^t\left(\xi_1\mathrm{sig}^{\alpha_1}\left(\eta_e\right)+\xi_2\mathrm{sig}^{\alpha_2}\left(\omega_e\right)\right)\mathrm{d}s \tag{57}$$

where ξ_1,ξ_2 are positive real numbers, $0<\alpha_1<1$, $\alpha_2=2\alpha_1/\left(\alpha_1+1\right)$.

The FTSMC control law is given by:

$$\tau=J^{\mathrm{T}}(\eta)\left(-K_1s-K_2\mathrm{sig}^{\mu}(s)-\beta\,\mathrm{sgn}(s)\right) \tag{58}$$

The AI-FTSMC control law is given by:

$$\tau=J^{\mathrm{T}}(\eta)\left(-K_1s-K_2\mathrm{sig}^{\mu}(s)-\frac{\hat{b}\vartheta}{\|s\|+\gamma}s\right) \tag{59}$$

where K_1 and K_2 are positive definite diagonal matrices, $0<\mu<1$, $\gamma=\dfrac{\varphi}{1+\vartheta}$, φ is a positive constant, and $\hat{b}$ satisfies $\dot{\hat{b}}=-\zeta_1\hat{b}+\zeta_2\dfrac{\|s\|^2\vartheta}{\|s\|+\gamma}$, $\vartheta=1+\dot{\eta}+\dot{\eta}^2+\dot{\eta}^3+\dot{\eta}^{\alpha_2}$.

To ensure the fairness of the comparisons among the different control methods, all the simulations were conducted under identical conditions, including the same USV model parameters, initial states, reference trajectories, and external disturbances. The controller parameters were tuned such that the control input magnitudes of all methods remained within a comparable range, ensuring that no controller benefited from greater control authority. The parameter selections for each control method are as follows: For the FTSMC and AI-FTSMC control parameters in Equations (57)-(59), the values are given as $\xi_1=20.8$, $\xi_2=12$, $\alpha_1=0.9$, $K_1=\mathrm{diag}[20,20,20]$, $K_2=\mathrm{diag}[10,10,10]$, $\mu=0.9$, $\zeta_1=2$, $\zeta_2=0.01$. The control parameters related to Adaptive PT-NTSMC in this paper are given as: $b=0.005$, $\kappa=0.008$, $\alpha=27/19$, $\alpha_1=0.9$, $\delta=4.1$, $T=T_c$, $\varsigma=0.5$. It can be obtained by solving the system of equations (41) that $a=\mathrm{diag}(2.8718,3.1099,1.8146)$, $\chi=[-0.0799,0.0904,-0.0248]^{\mathrm{T}}$.

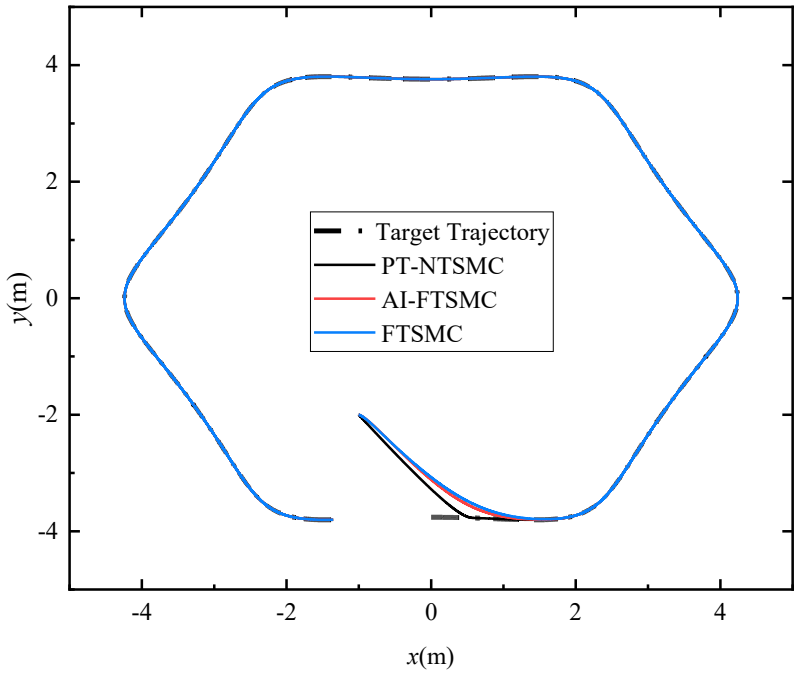

Fig. 4 3-DOF USV trajectory tracking performance

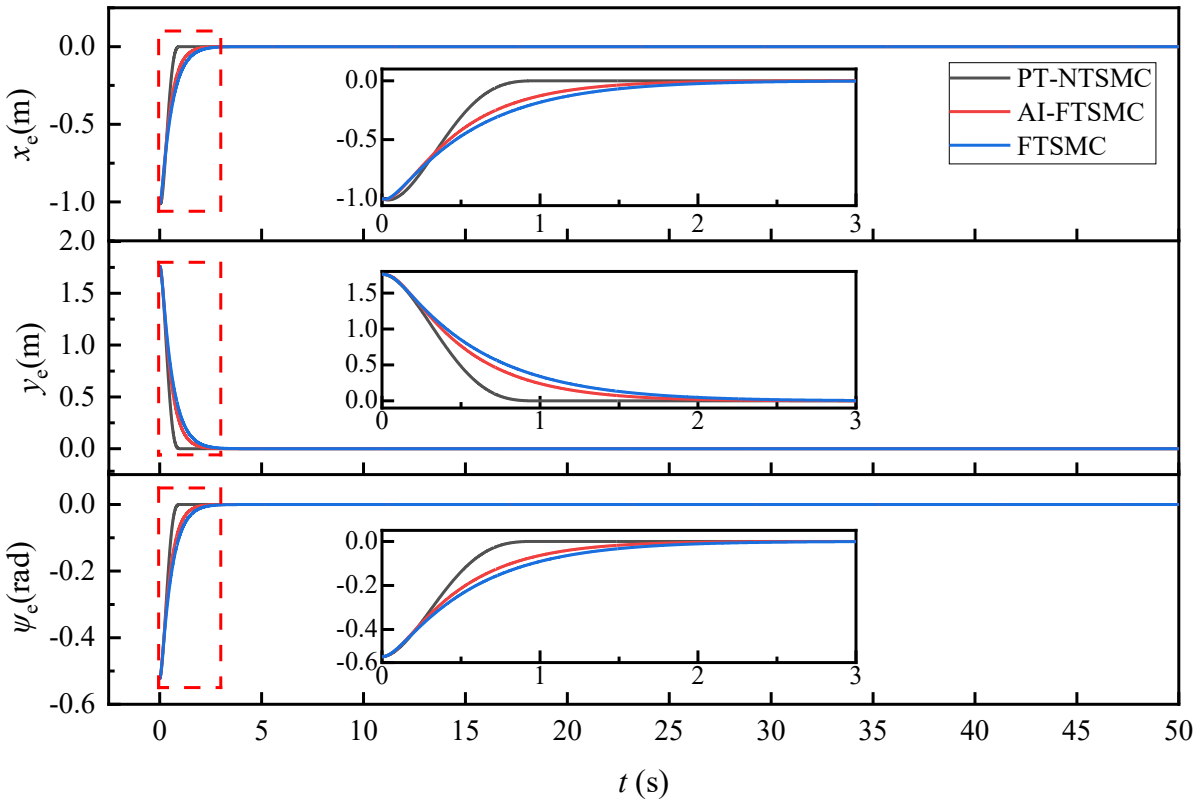

Fig. 5 Comparison of 3-DOF position tracking errors

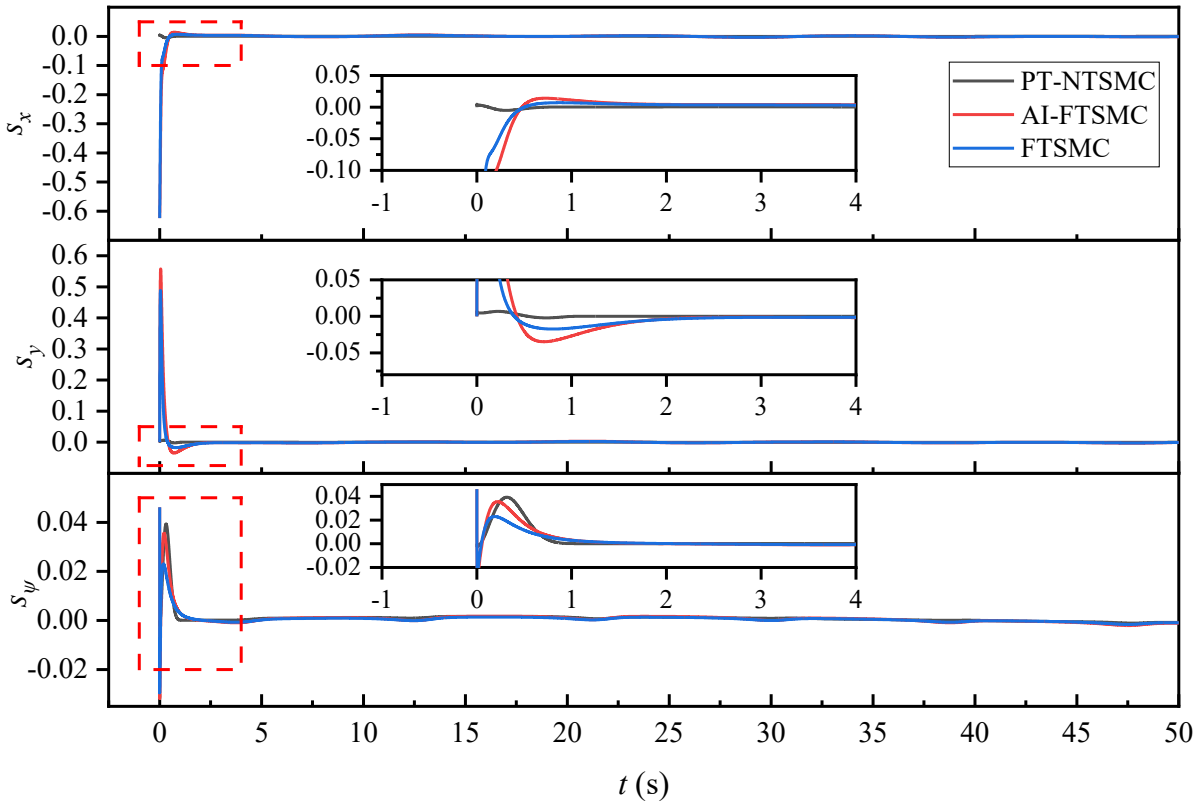

Fig. 6 3-DOF sliding mode manifold

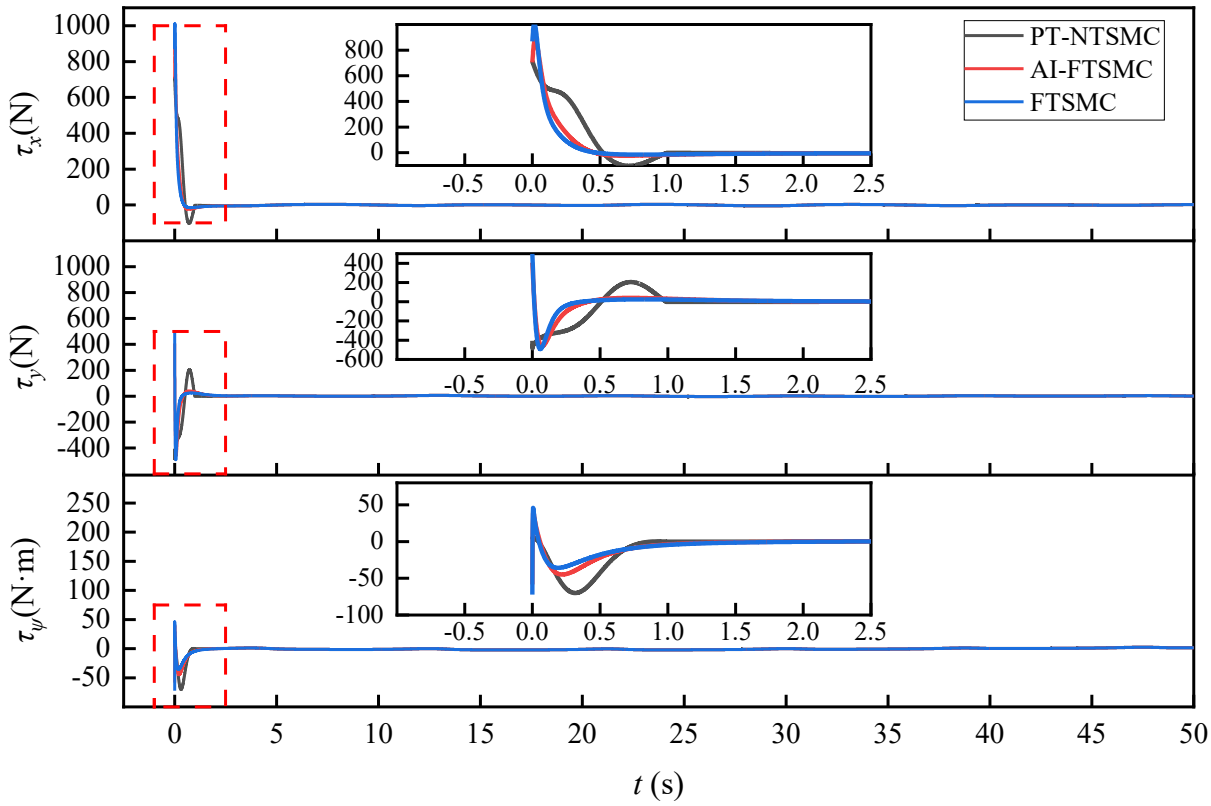

Fig. 7 Comparison of 3-DOF control inputs

Comparisons of the simulation results of PT-NTSMC, AI-FTSMC, and FTSMC are presented in Figures 4-7. As shown in Figure 4, all three methods successfully track the given irregular trajectory. However, the PT-NTSMC method proposed in this paper allows the USV's trajectory to merge with the target trajectory at a position further ahead along the path, indicating that the USV can travel a longer distance along the target trajectory. This helps improve the task completion rate while reducing cumulative errors throughout the mission. As shown in Figure 4, the PT-NTSMC method achieves faster trajectory tracking, enabling the USV to reach the target trajectory earlier. It is evident that the tracking error converges to zero within the given predefined time of 1 second and remains at zero thereafter, demonstrating the predefined time stability of the PT-NTSMC method. The sliding mode function curve in Figure 6 shows that the PT-NTSMC method ensures that the system state remains on the sliding mode surface from the initial stage and throughout the control process. This finding indicates that the proposed controller effectively eliminates the reaching phase, thereby enhancing system robustness.

Table 2 IAE values of 3-DOF for each controller

	IAE_x (m)	IAE_y (m)	IAE_ψ (rad)
PT-NTSMC	0.4090	0.6701	0.2006
AI-FTSMC	0.5402	0.9785	0.2748
FTSMC	0.6176	1.1188	0.3142

Table 3 ITAE values of 3-DOF for each controller

	$ITAE_x$ (m)	$ITAE_y$ (m)	$ITAE_\psi$ (rad)
PT-NTSMC	0.1078	0.1690	0.1444
AI-FTSMC	0.2525	0.4563	0.1544
FTSMC	0.3403	0.6218	0.1893

To further analyze the control performance of each method, the IAE and ITAE values corresponding to each control approach are presented in Tables 2 and 3, which are calculated using the equations $\mathrm{IAE}=\int_0^t|\eta_e(s)|ds$ and $\mathrm{ITAE}=\int_0^t s|\eta_e(s)|ds$ [58]. Compared with the other two methods, PT-NTSMC achieves lower IAE and ITAE values across all degrees of freedom, indicating that the proposed controller exhibits superior steady-state and transient performance.

To further validate the effectiveness of PT-NTSMC, simulation studies are conducted to evaluate its trajectory tracking performance under different initial positions and predefined times. Five cases with different initial positions are designated as Cases 1-5, while five cases with different predefined times are labeled as Cases 1, and 6-9. The detailed simulation results and analysis are presented below:

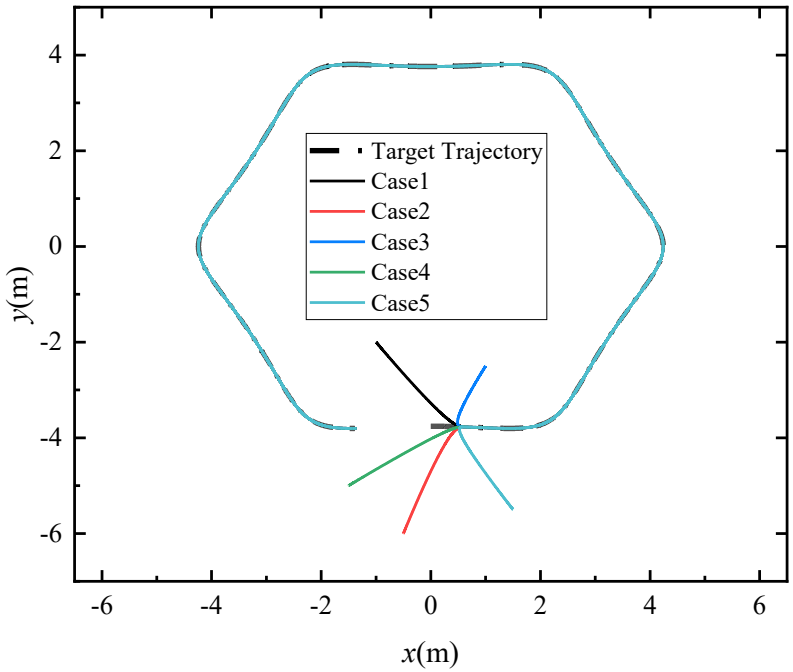

Fig. 8 USV motion trajectories under different initial positions

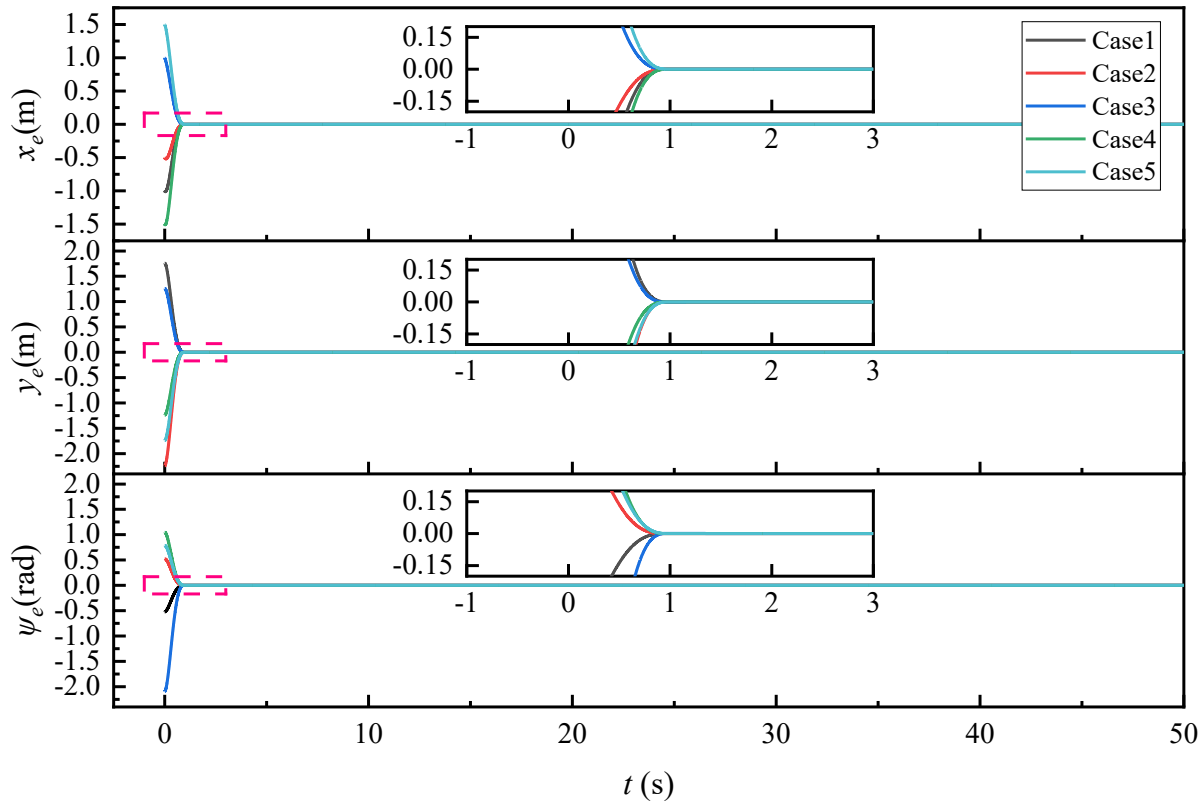

Fig. 9 Position tracking error under different initial positions

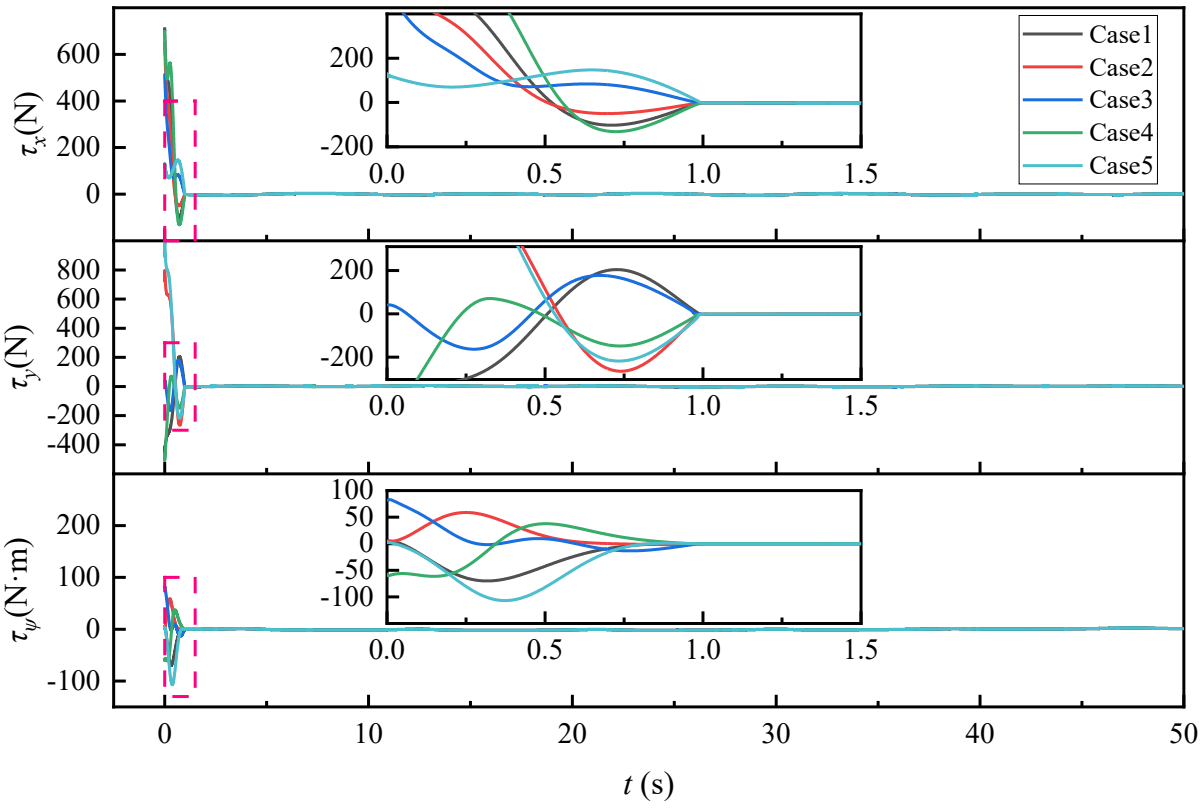

Fig. 10 Control inputs under different initial positions

The study of the controller's performance for different initial positions includes 5 cases, which are as follows: Case 1: $\eta_0 = [-1, -2, -\pi/6]^{\mathrm{T}}$, Case 2: $\eta_0 = [-0.5, -6, \pi/6]^{\mathrm{T}}$, Case 3: $\eta_0 = [1, -2.5, -2\pi/3]^{\mathrm{T}}$,

Case4: $\eta_0 = [-1.5, -5, \pi/3]^{\mathrm{T}}$, Case 5: $\eta_0 = [1.5, -5.5, \pi/4]^{\mathrm{T}}$. The predefined time parameter is set to $T = 1$ s.

From Figures 8-10, it can be observed that for any initial position, the USV is able to accurately converge to the target trajectory within the predefined time. This finding demonstrates that the proposed PT-NTSMC method ensures predefined time convergence, even under different initial conditions. Despite larger initial deviations of the USV, its ability to reach the target trajectory on time is unaffected. Moreover, once the USV reaches the target trajectory, its motion remains stable, and it continues to track the target trajectory smoothly without overshoot or oscillations. This further validates the effectiveness and stability of the designed controller. From Figure 10, it is evident that the control input changes smoothly, without sharp jumps or high-frequency chattering. This finding indicates that the adopted control method not only guarantees that the USV completes the trajectory tracking task within the predefined time but also ensures a smoother control input, avoiding the chattering issues commonly seen in sliding mode control. This is particularly important for practical applications, since it helps reduce actuator burden and improves the operational feasibility and safety of the system. In conclusion, the simulation results show that the proposed control method ensures that the USV reaches the target trajectory within the predefined time under different initial positions while maintaining stable operation during subsequent tracking. Additionally, the control input variations are smooth, with no noticeable chattering, further demonstrating the feasibility and superiority of the method in engineering applications.

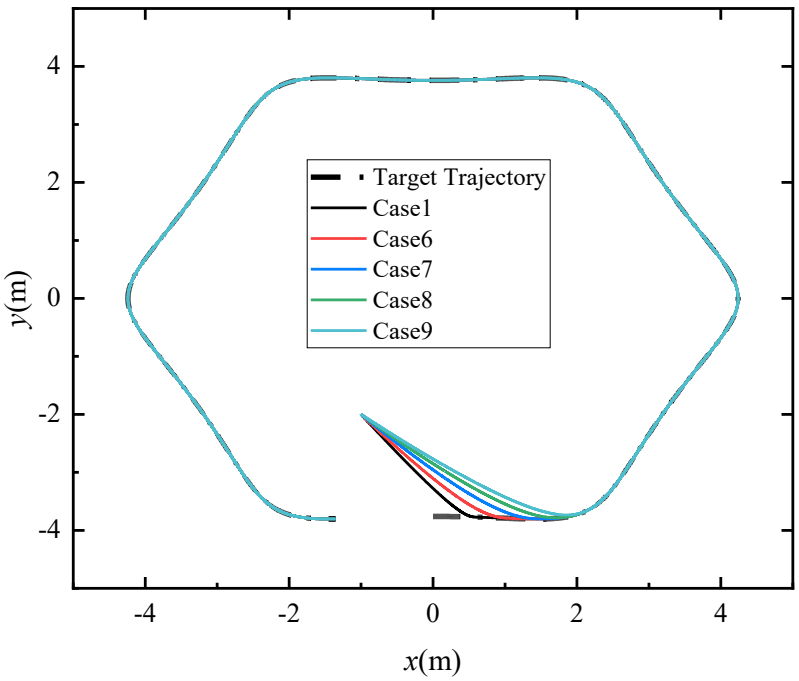

Fig. 11 USV motion trajectories under different predefined times

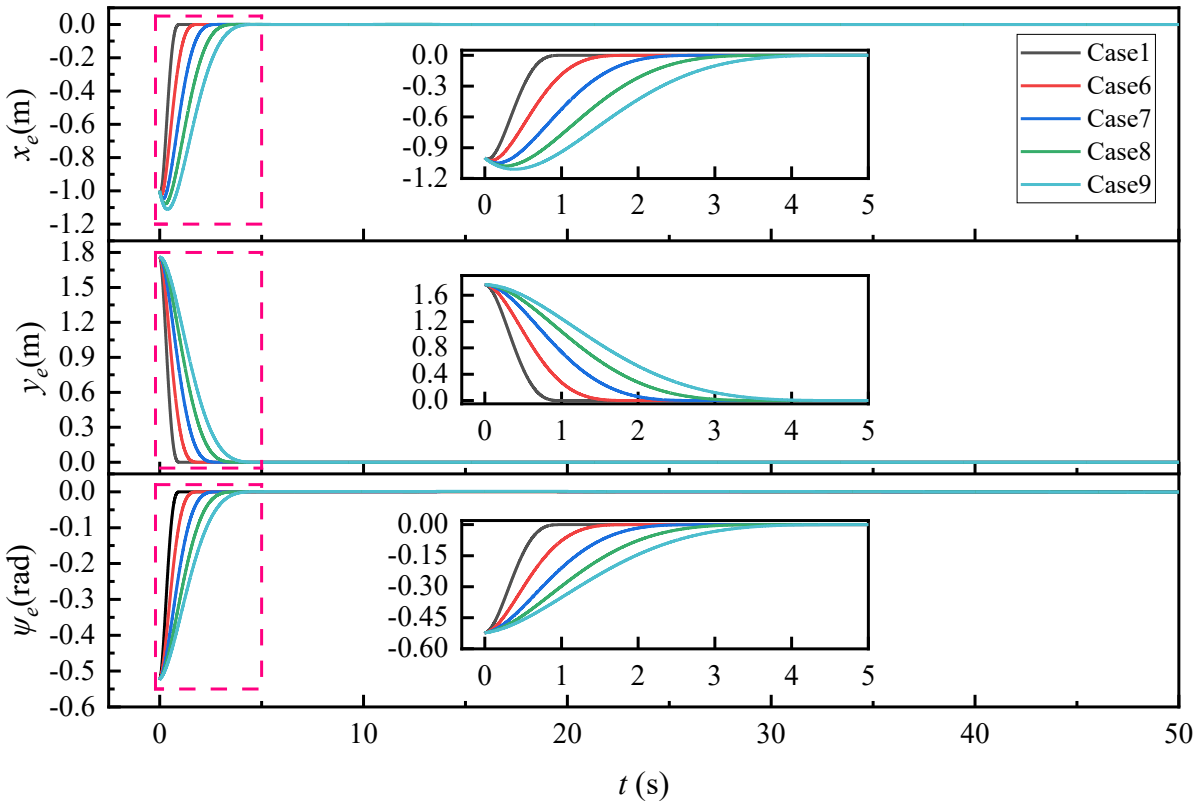

Fig. 12 Tracking error under different predefined times

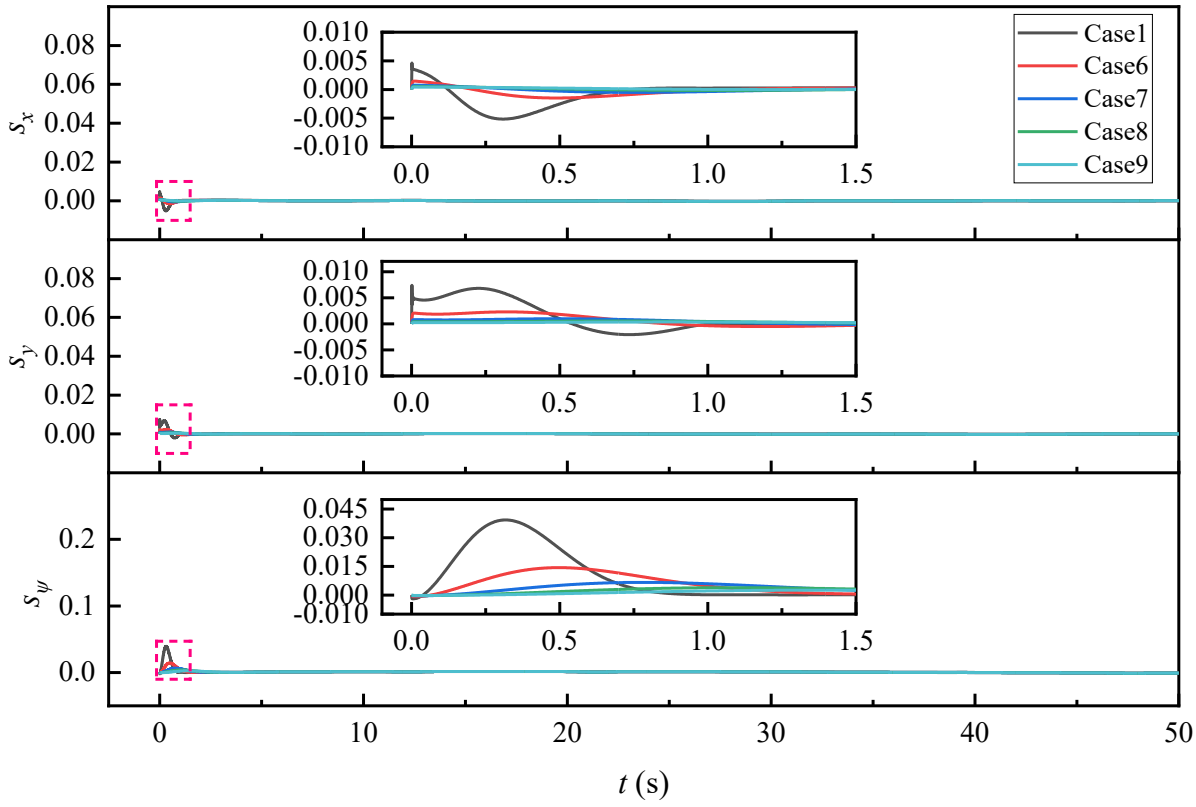

Fig. 13 Sliding mode manifolds under different predefined times

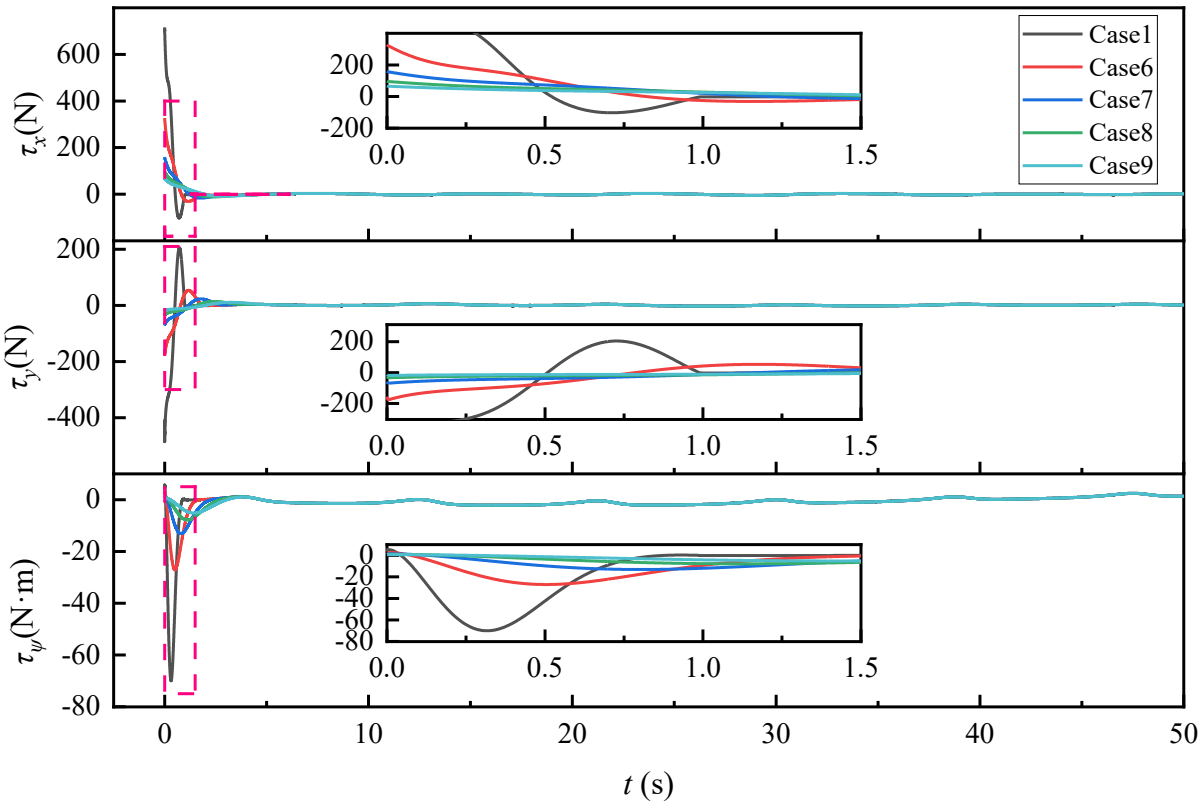

Fig. 14 Control inputs under different predefined times

The study of trajectory tracking performance under different predefined times includes five cases, which are as follows: Case 1: $T = 1$ s, Case 6: $T = 2$ s, Case 7: $T = 3$ s, Case 8: $T = 4$ s, Case 9: $T = 5$ s. The initial position for all cases is $\eta_0 = [-1, -2, -\pi/6]^{\mathrm{T}}$.

As shown in Figures 11-14, it can be seen that the USV is able to reach the target trajectory and perform accurate trajectory tracking within the given predefined times. Notably, as shown in Figure 12, when the predefined time parameter is larger, the tracking error in the x-direction first increases but then decreases. This is because at the initial moment, the USV's velocity is zero, whereas the target trajectory's velocity in the x-direction is greater than that of the USV. Given the larger predefined-time parameter, the system responds with a relatively smaller initial acceleration, and therefore the tracking error increases first before decreasing. However, as the USV velocity increases, the tracking error decreases accordingly. From Figure 13, it is evident that the system state remains on the sliding mode surface throughout the process. Therefore, the controller effectively suppresses external disturbances during the entire control process, thereby enhancing the system's robustness.

5.2 Control performance of the adaptive predefined time nonsingular terminal sliding mode controller

In this section, the adaptive PT-NTSMC designed in Section 4.2 is used to simulate and analyze the trajectory tracking performance of a USV under unknown external disturbance bounds and input saturation.

In practical applications, the actuators of an USV are subject to physical constraints. If the control input exceeds the feasible range of the actuator, saturation effects may occur, leading to discrepancies between the control input and the theoretically calculated values. In such cases, the dynamic response of the USV may deviate from the expected behavior, and the stability and convergence rate of the system could be affected. This could result in the USV failing to follow the controller's instructions accurately. Therefore, when the controller is designed, it is essential to consider the impact of input saturation to ensure that the generated control inputs remain within the feasible range of the actuators.

According to reference [59], the limitation of control force is given as $|\tau| \le \tau_{\lim i}\ i=1,2$, and $\tau_{\lim i}=50$ N , and the limitation of the control torque is given as $|\tau| \le \tau_{\lim i}\ i=3$, and $\tau_{\lim i}=30$ Nm . To avoid abrupt changes in control inputs under input saturation, the following function is chosen to achieve smooth variations in the control inputs:

$$\Gamma(\tau_i)=\tau_{\lim i}\operatorname{sign}(\tau_i)\tanh\left(\frac{\tau_i}{\tau_{\lim i}\operatorname{sign}(\tau_i)}\right) \tag{60}$$

In this section, the relevant parameters are set as follows: $\eta_0=[-1,-2,-\pi/6]^{\mathrm{T}}$, $T=3$ s .

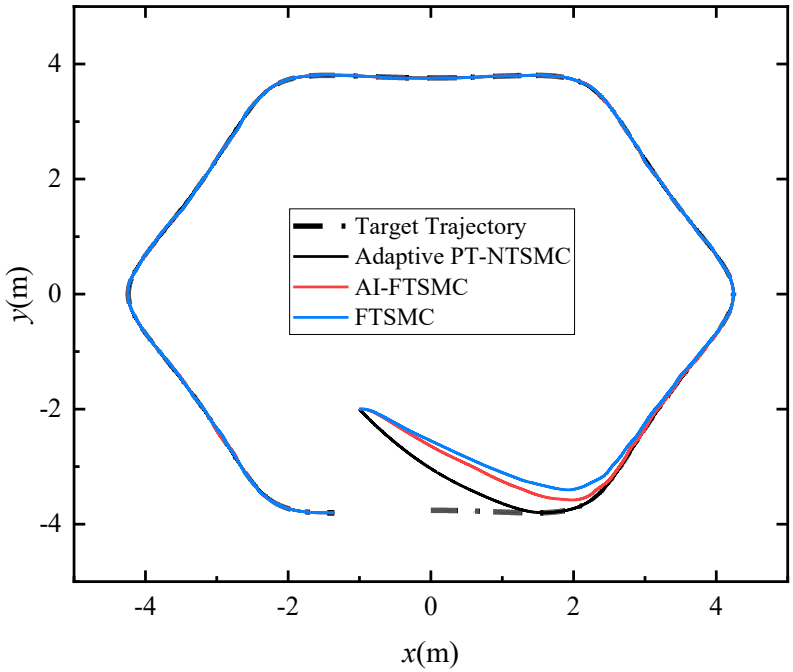

Fig. 15 USV motion trajectory

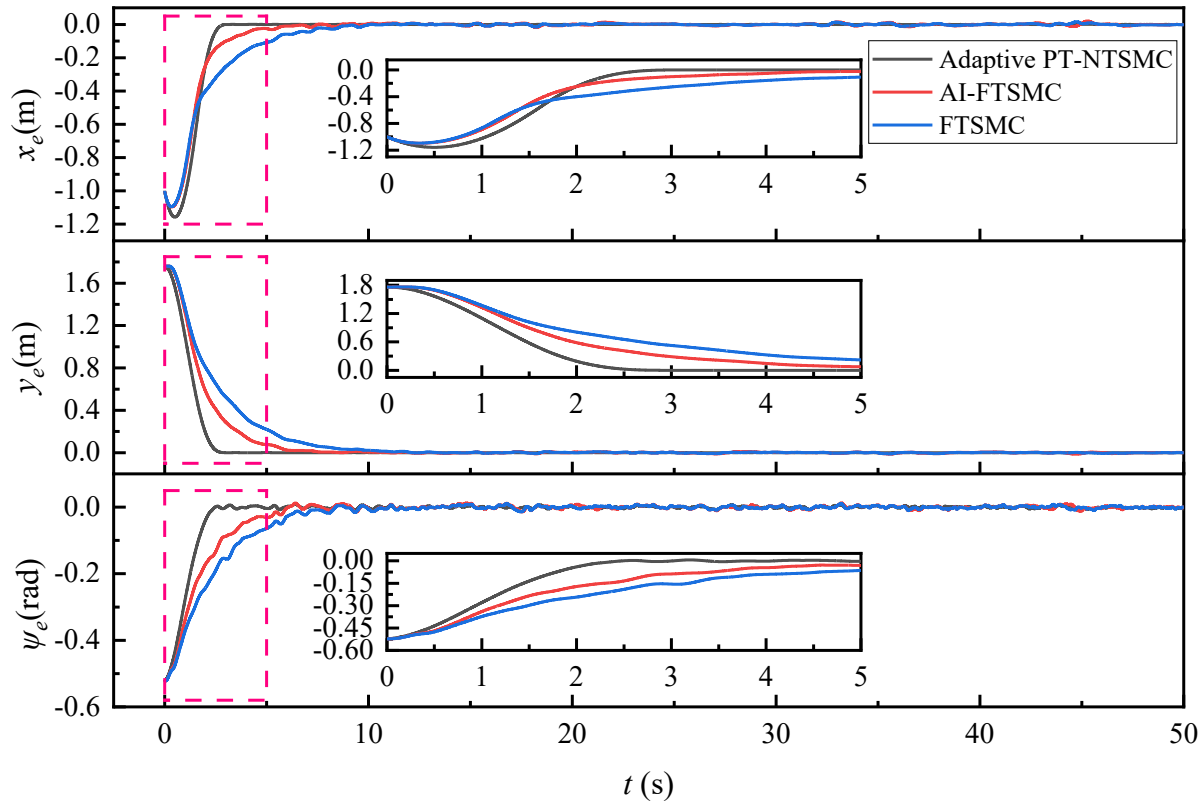

Fig. 16 Position tracking error

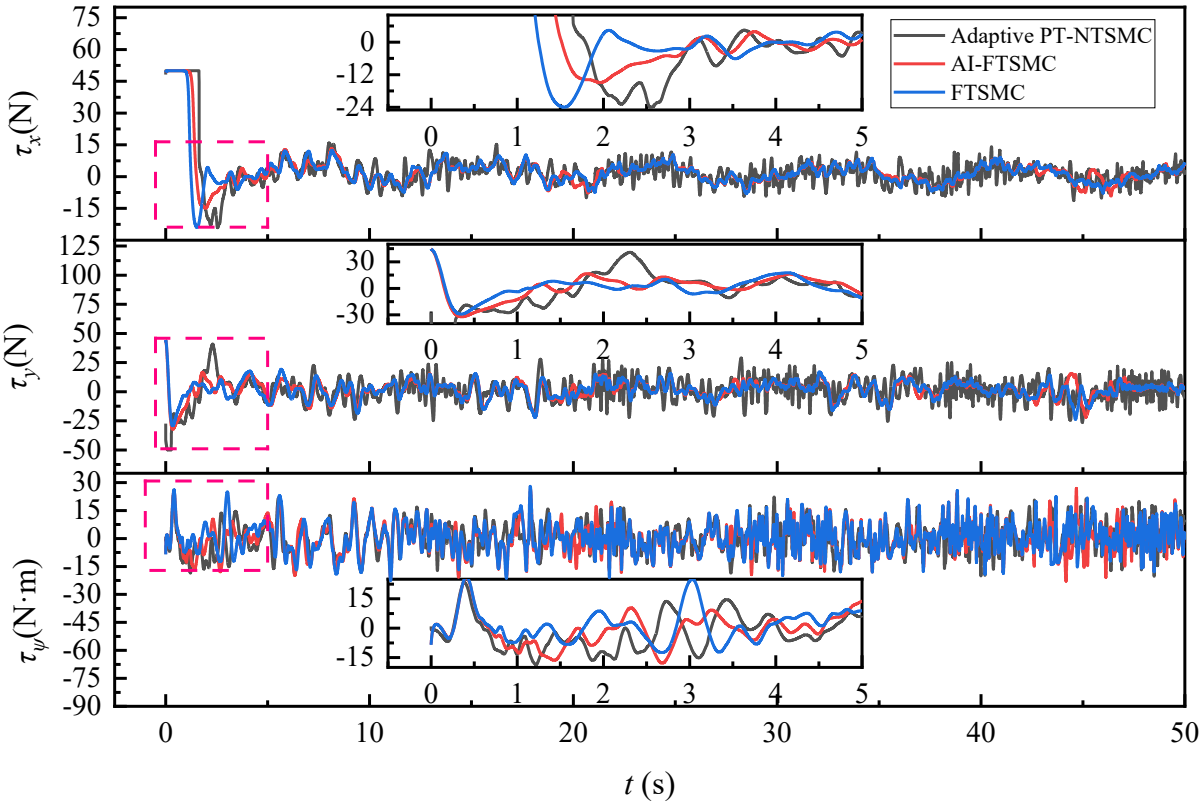

Fig. 17 Control inputs

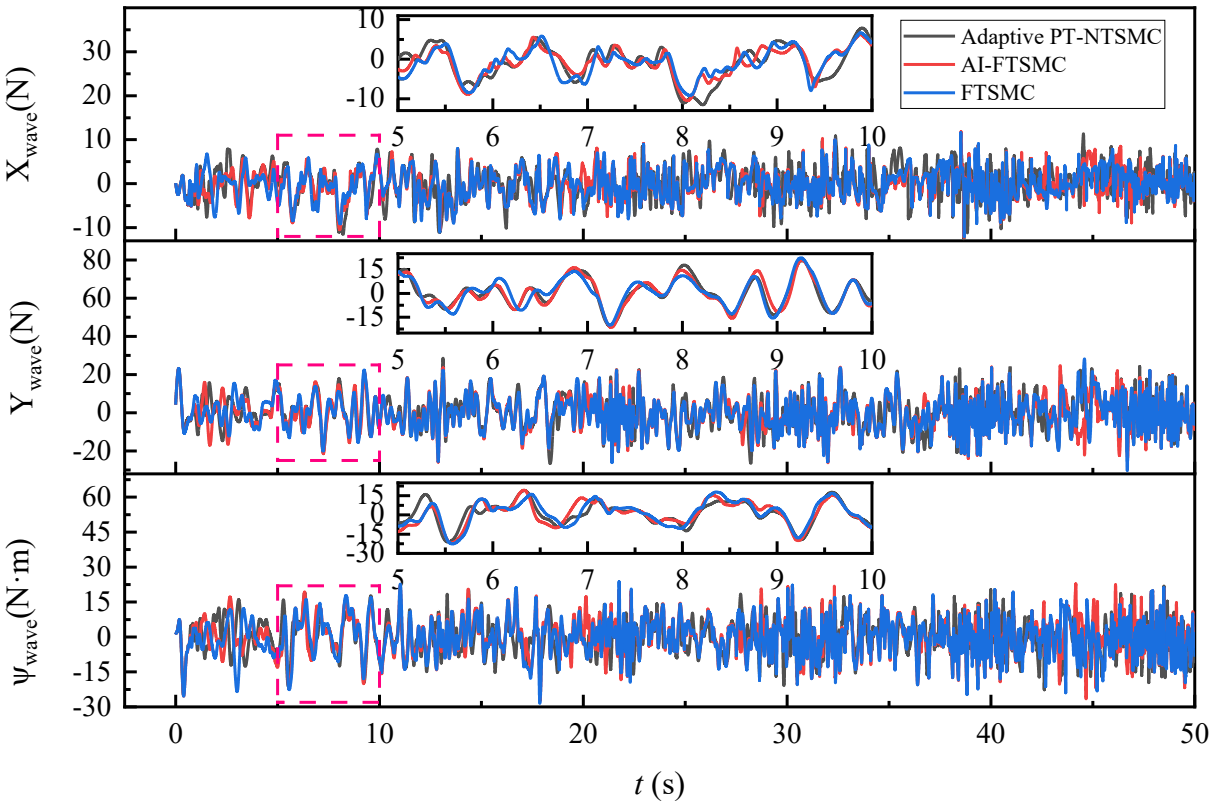

Fig. 18 Wave disturbance

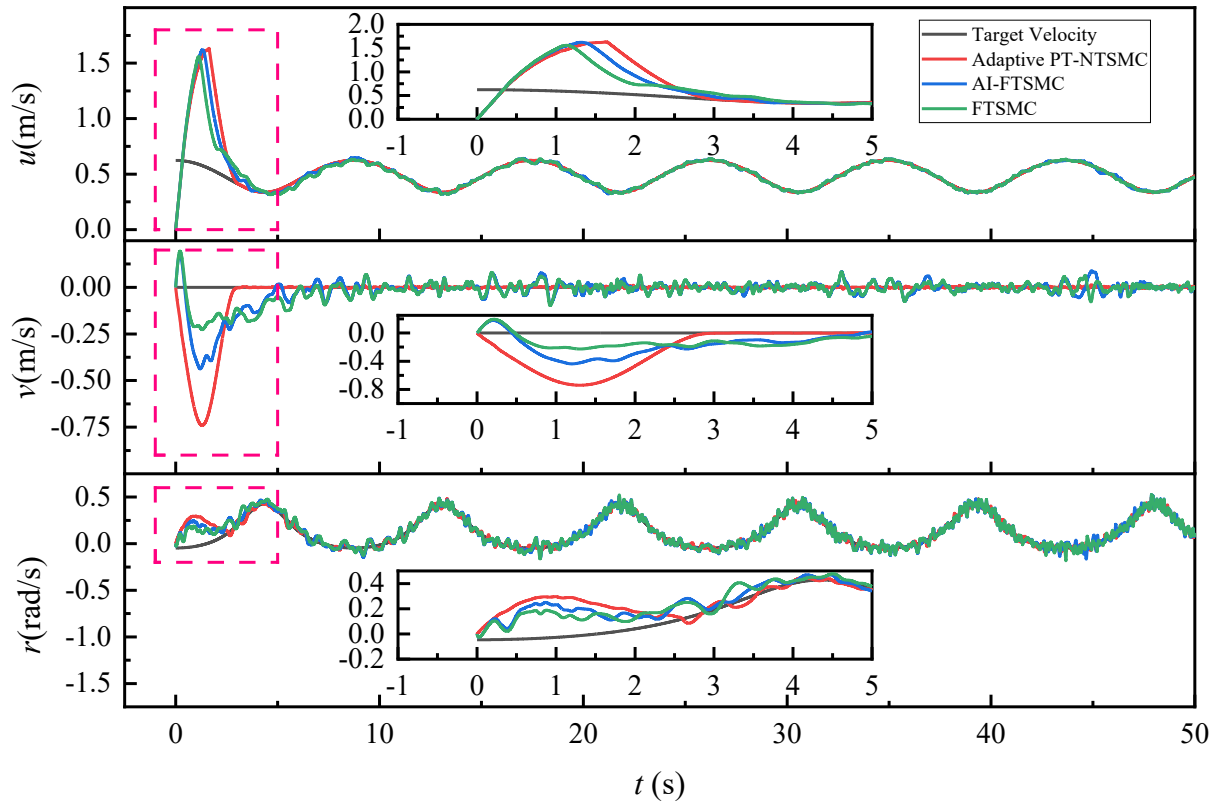

Fig. 19 Velocity

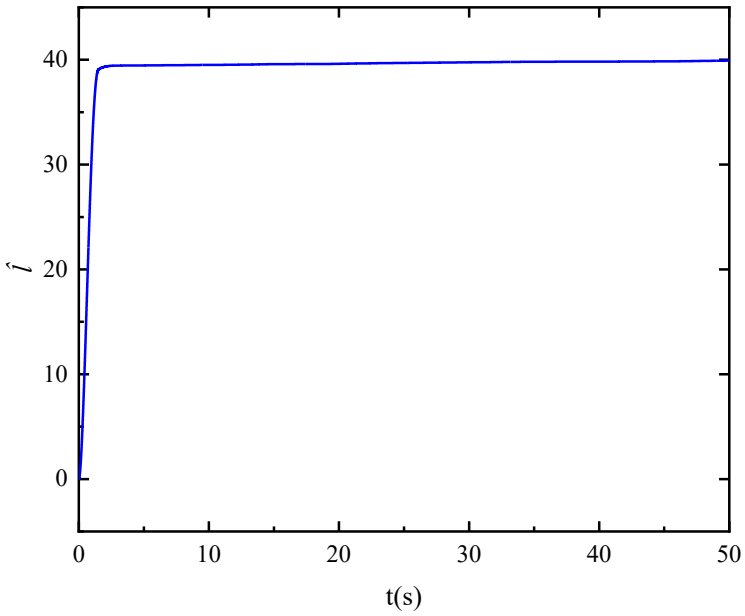

Fig. 20 Adaptive parameter

The comparative results of the adaptive PT-NTSMC and the two benchmark methods under input saturation constraints. are presented in Figures 15-20. Compared with the AI-FTSMC and FTSMC methods, the adaptive PT-NTSMC method achieves superior tracking performance, featuring faster error attenuation, smaller steady-state errors, and more stable USV velocity responses. In Figure 16, the position tracking error curves of all three methods are plotted together. Notably, the predefined time parameter T=3 s is associated with the proposed Adaptive PT-NTSMC. The corresponding error curve converges within 3 s, whereas the AI-FTSMC and FTSMC methods converge more slowly, demonstrating the convergence speed advantage of the proposed method. As shown in Figure 18, the wave-induced forces corresponding to different control methods exhibit slight discrepancies. This is because the magnitude of the wave forces depends on the USV's velocity and heading angle. Under the three control methods, the USV velocities vary slightly over time, which consequently leads to differences in the resulting wave-induced forces. The curve of adaptive parameter over time. is shown in Figure 20. The adaptive parameters undergo dynamic adjustments before reaching the predefined time and stabilize at a constant value afterward. This phenomenon validates the effectiveness of the designed adaptive law, demonstrating that the system can adaptively adjust the control gain to ensure accurate trajectory tracking and system stability, even in the presence of unknown external disturbances and input saturation.

Table 4 IAE values of 3-DOF for each controller

	IAE_x (m)	IAE_y (m)	IAE_ψ (rad)
Adaptive PT-NTSMC	1.8384	2.1783	0.6897
AI-FTSMC	2.0597	3.5500	1.1182
FTSMC	2.5965	4.5991	1.3729

Table 5 ITAE values of 3-DOF for each controller

	$ITAE_x$ (m)	$ITAE_y$ (m)	$ITAE_\psi$ (rad)
Adaptive PT-NTSMC	1.8263	1.8144	3.1989
AI-FTSMC	7.6079	9.6838	5.7403
FTSMC	9.0765	13.1650	6.0839

Quantitative comparisons based on the IAE and ITAE indices are summarized in Tables 4 and 5. As shown in Table 4, the proposed adaptive PT-NTSMC achieves the smallest IAE values for all three DOFs.

Compared those of the with AI-FTSMC, the IAE_x, IAE_y, and IAE_ψ of the adaptive PT-NTSMC are reduced by approximately 10.7 %, 38.6 %, and 38.3 %, respectively. Compared with the conventional FTSMC, the corresponding reductions reach 29.2 %, 52.6 %, and 49.8 %, respectively, for the adaptive PT-NTSMC. These results indicate that the proposed method significantly improves tracking accuracy in terms of both position and heading. Table 5 shows the ITAE results. Compared with AI-FTSMC, the $ITAE_x$, $ITAE_y$, and $ITAE_\psi$ achieved by the adaptive PT-NTSMC are reduced by approximately 76.0 %, 81.3 %, and 44.3 %, respectively. Compared with those of FTSMC, the reductions further increase to 79.9 %, 86.3 %, and 47.4 %, respectively, in the adaptive PT-NTSMC. A smaller ITAE indicates a reduced error magnitude in the later stage of the tracking process and a lower residual error, demonstrating improved late-stage performance under input saturation.

6. Conclusion

In this paper, a predefined time trajectory tracking control framework for USVs under realistic wave disturbances is developed. By incorporating a short-crested irregular wave force model into the control-oriented dynamic framework, the proposed method provides a more physically realistic representation of wave disturbances and the reliability of simulation-based evaluation. A novel time-varying function was further introduced to construct a variable-gain predefined time sliding mode manifold, through which the reaching phase is eliminated and predefined time convergence of the tracking error was achieved. On this basis, an adaptive PT-NTSMC is proposed by embedding an online estimation law of the upper bound of the disturbance into the predefined time sliding mode framework, thereby strengthening disturbance rejection capability under wave disturbances. Comparative simulation results demonstrated that the proposed method provides more accurate trajectory tracking and more stable velocity responses than the AI-FTSMC and conventional FTSMC methods do. Although input saturation is considered in the present study, the dynamic characteristics of the thrusters, such as response-speed limitations and actuator lag, are not explicitly incorporated. In future work, the proposed control framework will be extended to include actuator dynamics so as to further improve its engineering realism.

ACKNOWLEDGEMENTS

This work was supported by the National Key Research and Development Program (2022YFC2805200); China COSCO Shipping Corporation Limited (2023-2-Z001-02-01); the Natural Science Foundation of Liaoning Province (2024-MS-016); and the Fundamental Research Funds for the Central Universities (3132025617).

REFERENCES

[1] Dong, Z., Lu, S., Hu, Z., Liu, W., Ding, Y., Liu, Y., 2025. Simultaneous modeling and backstepping control algorithm for trajectory tracking of underactuated USV based on real-time sailing data in complex ocean conditions. *ISA Transactions,* 166, 145-158. https://doi.org/10.1016/j.isatra.2025.07.013

[2] Wei, J., Zhang, J., Dong, H., Liu, Z., 2025. Prescribed-time trajectory tracking control for underactuated USV with input amplitude and rate constraints. *Ocean Engineering,* 326, 120891. https://doi.org/10.1016/j.oceaneng.2025.120891

[3] Xu, W., Zhang, X., Miao, Z., 2025. Cooperative trajectory tracking control of USV-UAV with non-singular sliding mode surface and RBF neural network. *Ocean Engineering,* 337, 121872. https://doi.org/10.1016/j.oceaneng.2025.121872

[4] Mu, D., Lang, Z., Fan, Y., Zhao, Y., Zhu, G., Gao, Y., 2024. Trajectory tracking control of unmanned surface vehicle based on optimized barrier Lyapunov function under real ocean wave modeling. *Journal of the Franklin Institute,* 361(16), 107182. https://doi.org/10.1016/j.jfranklin.2024.107182

[5] Guan, W., Xi, Z. Y., Cui, Z. W., Zhang, X. K., 2025. Adaptive trajectory controller design for unmanned surface vehicles based on SAC-PID. *Brodogradnja,* 76(2), 76206. https://doi.org/10.21278/brod76206

[6] Zhao, Q. S., Peng, C., Mu, C. X., Li, S. C., Li, D. J., 2026. Robust trajectory tracking of surface vessels in ice floe sea state via discrete integral sliding-mode control and Gaussian process regression. *Brodogradnja,* 77(2), 77206. https://doi.org/10.21278/brod77206

[7] Zhang, Y., Zhang, J. N., Guo, Z. Y., Zhang, L., Shang, Y. C., 2025. An adaptive NMPC for ROVs trajectory tracking with environmental disturbances and model uncertainties. *Brodogradnja,* 76(1), 76106. https://doi.org/10.21278/brod76106

[8] Zhu, G. B., Ma, Y., Hu, S. L., 2025. Event-Sampled Adaptive Fuzzy Control of MASS via Intermittent Position Data. *IEEE Transactions on Emerging Topics In Computational Intelligence*. https://doi.org/10.1109/TETCI.2025.3526331

[9] Huang, B., Ren, X., Zhou, B., Zhang, Z., Zhou, X., Miao, J., 2025. An Intermittent Anti-Competition Communication Mechanism-Based Formation Maneuvers for Internet of Unmanned Surface Vehicles. *IEEE Internet of Things Journal,* 12(3), 3234-3247. https://doi.org/10.1109/JIOT.2024.3478784

[10] Meng, Y. H., Ye, H., Xiang, Z. R., Yang, X. F., Zhang, H., 2024. An adaptive internal model control approach for unmanned surface vehicle based on bidirectional long short-term memory neural network: Implementation and field testing. *Mechatronics,* 99, 103145. https://doi.org/10.1016/j.mechatronics.2024.103145

[11] Zhao, G., Chen, Z., Liao, W., 2024. Reinforcement-Tracking: An End-to-End Trajectory Tracking Method Based on Self-Attention Mechanism. *International Journal of Automotive Technology,* 25(3), 541-551. https://doi.org/10.1007/s12239-024-00043-5

[12] Shin, G. H., Yang, H., 2025. Deep reinforcement learning for integrated vessel path planning with safe anchorage allocation. *Brodogradnja,* 76(3), 76305. https://doi.org/10.21278/brod76305

[13] Zhang, L., Chen, L., Saqib, M., Wang, B., Xu, P., Zhao, Y., 2025. An integral terminal sliding mode-based adaptive control approach for traversing unknown inclined surfaces. *Robotics and Autonomous Systems,* 186, 104928. https://doi.org/10.1016/j.robot.2025.104928

[14] Rinaldi, M., Primatesta, S., Guglieri, G., 2023. A Comparative Study for Control of Quadrotor UAVs. *Applied Sciences,* 13(6), 3464. https://doi.org/10.3390/app13063464

[15] Nasr, M., Ashraf, M., Hussein, M. S., Salem, A. S., Elias, C. M., Shehata, O. M., Morgan, E. I., 2018. A comparitive study on the control of UAVs for Trajectory tracking by MPC, SMC, Backstepping, and Fuzzy Logic controllers, *2018 IEEE International Conference on Vehicular Electronics and Safety (ICVES)*, 12-14 September, Madrid, Spain. https://doi.org/10.1109/ICVES.2018.8519511

[16] Gan, W., Zhu, D., Ji, D., 2018. QPSO-model predictive control-based approach to dynamic trajectory tracking control for unmanned underwater vehicles. *Ocean Engineering,* 158, 208-220. https://doi.org/10.1016/j.oceaneng.2018.03.078

[17] Wen, Y., Chen, Y., Guo, X., 2024. USV Trajectory Tracking Control Based on Receding Horizon Reinforcement Learning. *Sensors,* 24(9). https://doi.org/10.3390/s24092771

[18] Close, J., Van, M., McIlvanna, S., 2024. PID-Fixed Time Sliding Mode Control for Trajectory Tracking of AUVs under Disturbance. *IFAC-PapersOnLine,* 58(20), 281-286. https://doi.org/10.1016/j.ifacol.2024.10.067

[19] Zhu, D., Yang, S. X., Biglarbegian, M., 2022. A Fuzzy Logic-based Cascade Control without Actuator Saturation for the Unmanned Underwater Vehicle Trajectory Tracking. *Journal of Intelligent & Robotic Systems,* 106(2), 39. https://doi.org/10.1007/s10846-022-01742-w

[20] Roxin, E., 1966. On finite stability in control systems. *Rendiconti del Circolo Matematico di Palermo,* 15(3), 273-282. https://doi.org/10.1007/BF02844106

[21] Rang, E., 1963. Isochrone families for second-order systems. *IEEE Transactions on Automatic Control,* 8(1), 64-65. https://doi.org/10.1109/TAC.1963.1105520

[22] Wang, N., Karimi, H. R., Li, H., Su, S. F., 2019. Accurate Trajectory Tracking of Disturbed Surface Vehicles: A Finite-Time Control Approach. *IEEE/ASME Transactions on Mechatronics,* 24(3), 1064-1074. https://doi.org/10.1109/TMECH.2019.2906395

[23] González-Prieto, J. A., 2023. Adaptive finite time smooth nonlinear sliding mode tracking control for surface vessels with uncertainties and disturbances. *Ocean Engineering,* 279, 114474. https://doi.org/10.1016/j.oceaneng.2023.114474

[24] Gao, L., Liu, X., Zong, G. D., Chen, Y. J., Shi, K. B., 2023. Finite-time sliding mode trajectory tracking control of an autonomous surface vehicle with prescribed performance. *Ocean Engineering,* 284, 114919. https://doi.org/10.1016/j.oceaneng.2023.114919

[25] Yang, Y., Cheng, S., Zeng, X., Liu, K., Li, T., 2025. Finite-time formation control of multi-USV systems with a relative-threshold event-triggered mechanism. *Ocean Engineering,* 341, 122614. https://doi.org/10.1016/j.oceaneng.2025.122614

[26] Huang, Y. W., Lai, G. Z., Lin, F., Shi, X. C., Li, D. F., 2025. Path Following With Finite-Time Convergence for Unmanned Surface Vehicle. *IEEE Journal Of Oceanic Engineering,* 50(2), 1153-1164. https://doi.org/10.1109/JOE.2024.3483328

[27] Liu, J., Wang, B. J. I. A., 2025. Adaptive fuzzy control of USV based on improved finite-time command-filtered backstepping method. *IEEE Access*. https://doi.org/10.1109/ACCESS.2025.3562579

[28] Zhang, X., Fan, Y., Dong, S., Shen, Z., Mu, D., Ye, X., Liu, P., 2026. Finite-time adaptive event-triggered control for USV trajectory tracking combined with intrinsic curiosity sequential proximal policy optimization. *Ocean Engineering,* 350, 124244. https://doi.org/10.1016/j.oceaneng.2026.124244

[29] Cruz-Zavala, E., Moreno, J. A., Fridman, L. M., 2011. Uniform Robust Exact Differentiator. *IEEE Transactions on Automatic Control,* 56(11), 2727-2733. https://doi.org/10.1109/TAC.2011.2160030

[30] Polyakov, A., 2012. Nonlinear Feedback Design for Fixed-Time Stabilization of Linear Control Systems. *IEEE Transactions on Automatic Control,* 57(8), 2106-2110. https://doi.org/10.1109/tac.2011.2179869

[31] An, S., Wang, L., He, Y., 2022. Robust fixed-time tracking control for underactuated AUVs based on fixed-time disturbance observer. *Ocean Engineering,* 266, 112567. https://doi.org/10.1016/j.oceaneng.2022.112567

[32] Shen, H., Yin, Y., Qian, X., 2022. Fixed-Time Formation Control for Unmanned Surface Vehicles with Parametric Uncertainties and Complex Disturbance. *Journal of Marine Science and Engineering,* 10(9), 1246. https://doi.org/10.3390/jmse10091246

[33] Meng, Y., Zhang, Y., Ye, H., Yang, X., Xiang, Z., 2025. Fixed-Time Tracking Control of Amphibious Unmanned Surface Vehicle: Theory and Experimentation. *IEEE Transactions on Industrial Electronics*, 1-11. https://doi.org/10.1109/TIE.2025.3639743

[34] Nie, J., Zhang, X., Wang, H., Sheng, C., Zhang, C., Zhang, C., 2025. Anti-saturation distributed fixed-time prescribed performance sliding mode formation control based on FXESO for uncertain USVs. *Ocean Engineering,* 318, 120101. https://doi.org/10.1016/j.oceaneng.2024.120101

[35] Yang, X. F., Wang, Q., Hu, J. B., Xu, B., Ding, S. H., Xiang, Z. R., Zhang, B., 2025. Fixed-Time Generalized Super-Twisting Controller for the Trajectory Tracking of Unmanned Surface Vehicles in Autonomous Berthing. *IEEE Transactions On Industrial Electronics,* 72(5), 5300-5311. https://doi.org/10.1109/TIE.2024.3468648

[36] Yan, Y., Yin, C., Hou, Y., Yu, S., Liu, Y., 2025. Adaptive fixed-time containment control of underactuated surface vessels with input quantization. *Ocean Engineering,* 318, 120157. https://doi.org/10.1016/j.oceaneng.2024.120157

[37] Wang, J.-B., Hao, L.-Y., Yang, X., 2024. Robust fixed-time fault-tolerant control for unmanned marine vehicles via integral terminal sliding mode technique. *Ocean Engineering,* 293, 116696. https://doi.org/10.1016/j.oceaneng.2024.116696

[38] Tong, H., Hu, Y., 2026. Global fixed-time prescribed performance control with fixed-time distributed state observer for non-cooperative target tracking using multiple unmanned surface vehicles. *ISA Transactions,* 168, 117-133. https://doi.org/10.1016/j.isatra.2025.11.033

[39] Su, Y. B., Yu, R. H., Ye, P. Y., Li, T. S., 2025. Singularity-Free Fixed-Time Cooperative Tracking Control of Unmanned Surface Vehicles with Model Uncertainties. *Journal Of Marine Science And Engineering,* 13(9), 1791. https://doi.org/10.3390/jmse13091791

[40] Meng, Y. H., Zhang, Y., Ye, H., Yang, X. F., Xiang, Z. R., 2024. Trajectory tracking control for unmanned amphibious surface vehicles with actuator faults. *Applied Ocean Research,* 152, 104182. https://doi.org/10.1016/j.apor.2024.104182

[41] Wang, Q., Yang, X. F., Hu, J. B., Ding, S. H., Shen, H., Xiang, Z. R., 2025. Fixed-Time Autonomous Berthing Control of Unmanned Surface Vehicles Under Output Constraints Based on Barrier Lyapunov Function. *IEEE Transactions On Intelligent Transportation Systems*. https://doi.org/10.1109/TITS.2025.3642626

[42] Sánchez-Torres, J. D., Sanchez, E. N., Loukianov, A. G., 2014. A discontinuous recurrent neural network with predefined time convergence for solution of linear programming, *2014 IEEE Symposium on Swarm Intelligence*, 9-12 December, Orlando, Florida, USA. https://doi.org/10.1109/SIS.2014.7011799

[43] Sánchez-Torres, J. D., Sanchez, E. N., Loukianov, A. G., 2015. Predefined-time stability of dynamical systems with sliding modes, *2015 American Control Conference (ACC)*, 1-3 July, Chicago, Illinois, USA. https://doi.org/10.1109/ACC.2015.7172255

[44] Zhang, Y., Liang, C.-D., Han, T., Yan, L., Ge, M.-F. J. I. T. o. V. T., 2026. A Novel Integrated Predefined-Time Distributed Coordination Framework for Networked Marine Surface Vehicles with Near-Optimal Path Determination Ability. *IEEE Transactions on Vehicular Technology*. https://doi.org/10.1109/TVT.2026.3669986

[45] Zhang, W., Xu, Y., Fu, M., Fan, Z., Dong, L., 2026. Data-driven predefined-time disturbance observer-based predictive control for hovercraft trajectory tracking. *Ocean Engineering,* 347, 124019. https://doi.org/10.1016/j.oceaneng.2025.124019

[46] Guo, G., Xiao, S., Shen, T., Chen, F., Guo, S., Luo, Z. J. N., 2026. Reinforcement learning predefined-time formation control for uncertain autonomous underwater vehicles with disturbance and input saturation. *Neurocomputing*, 133031. https://doi.org/10.1016/j.neucom.2026.133031

[47] Meng, Y., Zhang, Y., Ye, H., Yang, X., Xiang, Z., 2026. Prescribed-time fault-tolerant tracking control for aquatic-aerial unmanned amphibious vehicles. *Aerospace Science and Technology,* 168, 110872. https://doi.org/10.1016/j.ast.2025.110872

[48] Zhang, J., Yu, S., Yan, Y., 2020. Fixed-time velocity-free sliding mode tracking control for marine surface vessels with uncertainties and unknown actuator faults. *Ocean Engineering,* 201. https://doi.org/10.1016/j.oceaneng.2020.107107

[49] Ma, Y., Ning, J., Li, T., Liu, L., 2024. Distributed extended state observer based formation tracking control of under-actuated unmanned surface vehicles with input and state quantization. *Ocean Engineering,* 311, 118872. https://doi.org/10.1016/j.oceaneng.2024.118872

[50] Qiao, L., Zhang, W., 2017. Adaptive non-singular integral terminal sliding mode tracking control for autonomous underwater vehicles. *IET Control Theory & Applications,* 11(8), 1293-1306. https://doi.org/10.1049/iet-cta.2017.0016

[51] Su, Y., 2020. Comments on "A New Adaptive Sliding-Mode Control Scheme for Application to Robot Manipulators". *IEEE Transactions On Industrial Electronics,* 67(8), 7116-7120. https://doi.org/10.1109/TIE.2019.2939995

[52] Ahmed, S., Wang, H. P., Tian, Y., 2021. Adaptive High-Order Terminal Sliding Mode Control Based on Time Delay Estimation for the Robotic Manipulators With Backlash Hysteresis. *IEEE Transactions On Systems Man Cybernetics-Systems,* 51(2), 1128-1137. https://doi.org/10.1109/TSMC.2019.2895588

[53] Liu, M., Sun, D., Luo, F., Peng, E., 2024. Research on the Differences between Ocean Wave Parameters Retrieved Based on ITTC Spectra and PM Spectra, *2024 Photonics & Electromagnetics Research Symposium (PIERS)*, 21-25 April, Chengdu, China. https://doi.org/10.1109/PIERS62282.2024.10618704

[54] Umeda, N., Usada, S., Mizumoto, K., Matsuda, A., 2016. Broaching probability for a ship in irregular stern-quartering waves: theoretical prediction and experimental validation. *Journal of Marine Science and Technology,* 21(1), 23-37. https://doi.org/10.1007/s00773-015-0364-8

[55] Yu, S., Yu, X., Shirinzadeh, B., Man, Z., 2005. Continuous finite-time control for robotic manipulators with terminal sliding mode. *Automatica,* 41(11), 1957-1964. https://doi.org/10.1016/j.automatica.2005.07.001

[56] Skjetne, R., Fossen, T. I., Kokotovic, P. V., 2005. Adaptive maneuvering, with experiments, for a model ship in a marine control laboratory. *Automatica,* 41(2), 289-298. https://doi.org/10.1016/j.automatica.2004.10.006

[57] Yao, Q., 2020. Adaptive finite-time sliding mode control design for finite-time fault-tolerant trajectory tracking of marine vehicles with input saturation. *Journal of the Franklin Institute,* 357(18), 13593-13619. https://doi.org/10.1016/j.jfranklin.2020.10.015

[58] Wan, L., Cao, Y., Sun, Y., Qin, H., 2022. Fault-tolerant trajectory tracking control for unmanned surface vehicle with actuator faults based on a fast fixed-time system. *ISA transactions,* 130, 79-91. https://doi.org/10.1016/j.isatra.2022.04.013

[59] Dong, Z., Tan, F., Yu, M., Xiong, Y., Li, Z., 2024. A Bio-Inspired Sliding Mode Method for Autonomous Cooperative Formation Control of Underactuated USVs with Ocean Environment Disturbances. *Journal of Marine Science and Engineering,* 12(9), 1607. https://doi.org/10.3390/jmse12091607